https://doi.org/10.5194/nhess-2023-99
Preprint. Discussion started: 6 July 2023

Natural Hazards and Earth System Sciences
Discussions

High-resolution projections of ambient heat for major European cities using different heat metrics

Clemens Schwingshackl[1,2], Anne Sophie Daloz[2], Carley Iles[2], Kristin Aunan[2], Jana Sillmann[3,2]

[1]Department of Geography, Ludwig-Maximilians-Universität München, Munich, Germany
[2]Center for International Climate Research (CICERO), Oslo, Norway
[3]Center for Earth System Research and Sustainability (CEN), University of Hamburg, Hamburg, Germany

Correspondence to: Clemens Schwingshackl (c.schwingshackl@lmu.de)

Abstract. Heat stress in cities is projected to strongly increase due to climate change. The associated health risks will be exacerbated by the high population density in cities and the urban heat island effect. However, impacts are still uncertain, which is among other factors due to the existence of multiple metrics for quantifying ambient heat and the typically rather coarse spatial resolution of climate models. Here we investigate projections of ambient heat for 36 major European cities based on a recently produced ensemble of regional climate model simulations for Europe (EURO-CORDEX) at 0.11° spatial resolution (~12.5 km). The 0.11° EURO-CORDEX ensemble provides the best spatial resolution currently available from an ensemble of climate model projections for the whole of Europe and makes it possible to analyse the risk of temperature extremes and heatwaves at the city-level. We focus on three temperature-based heat metrics - yearly maximum temperature, number of days with temperatures exceeding 30 °C, and Heat Wave Magnitude Index daily (HWMId) - to analyse projections of ambient heat at 3 °C warming in Europe compared to 1981-2010 based on climate data from the EURO-CORDEX ensemble. The results show that southern European cities will be most affected by high levels of ambient heat, but depending on the considered metric, cities in central, eastern, and northern Europe may also experience substantial increases in ambient heat. In several cities, projections of ambient heat vary considerably across the three heat metrics, indicating that estimates based on a single metric might underestimate the potential for adverse health effects due to heat stress. Nighttime ambient heat, quantified based on daily minimum temperatures, shows similar spatial patterns as daytime conditions, albeit with substantially higher HWMId values. The identified spatial patterns of ambient heat are generally consistent with results from global Earth system models, though with substantial differences for individual cities. Our results emphasise the value of high-resolution climate model simulations for analysing climate extremes at the city-level. At the same time, they highlight that improving the currently rather simple representations of urban areas in climate models would make their simulations even more valuable for planning adaptation measures in cities. Further, our results stress that using complementary metrics for projections of ambient heat gives important insights into the risk of future heat stress that might otherwise be missed.

https://doi.org/10.5194/nhess-2023-99
Preprint. Discussion started: 6 July 2023

Natural Hazards and Earth System Sciences
Discussions

1 Introduction

Global heat stress is projected to strongly increase in the future due to climate change (Gasparrini et al., 2017; Vargas Zeppetello et al., 2022; Zheng et al., 2021; Schwingshackl et al., 2021; Freychet et al., 2022), and already nowadays record-breaking high temperatures are observed more and more often around the world, such as in Canada in summer 2021 or in China and Europe in summer 2022. Heat stress can have severe implications for human health, the economy, and the society as a whole (e.g., McMichael et al., 2006; Gasparrini et al., 2015; Yang et al., 2021; Alizadeh et al., 2022; Orlov et al., 2021), as it can lead to decreased levels of comfort and reduced labour productivity (Orlov et al., 2021; García-León et al., 2021), enhanced socioeconomic inequalities (Alizadeh et al., 2022), and increased morbidity and mortality (Gasparrini et al., 2015). Moreover, as the health risk associated with heat stress is not uniform within the population, heatwaves and extreme temperatures pose a larger threat to those who are most vulnerable to elevated temperatures, particularly to children, older adults, and persons with pre-existing conditions (Lundgren et al., 2013).

Various metrics have been developed with the aim to capture the characteristics of heat extremes, including heatwaves, and their potential evolution in the future (e.g., Perkins and Alexander, 2013; Perkins, 2015). Future changes in heat and heat extremes are frequently quantified by the change in temperature (e.g., mean or maximum near-surface air temperature) between a historical reference period and future periods (Sillmann et al., 2013; IPCC, 2021; Coppola et al., 2021). Other studies used the number of days per year during which certain thresholds are exceeded (e.g., Casanueva et al., 2020; Schwingshackl et al., 2021; Zhao et al., 2015). Likewise, different metrics have been introduced to quantify heatwaves, often based on percentile-based thresholds (e.g., Fischer and Schär, 2010; Suarez-Gutierrez et al., 2020; Perkins-Kirkpatrick and Lewis, 2020). The Heat Wave Magnitude Index daily (HWMId, Russo et al., 2015) integrates both the magnitude and the length of a heatwave into a single metric to quantify the heatwave severity. HWMId was applied by several studies to analyse the future risk of heatwaves (e.g., Dosio et al., 2018; Russo et al., 2017; Forzieri et al., 2016; Zittis et al., 2021). Depending on the considered metric, the projected spatial patterns of ambient heat projections may vary considerably, highlighting that assessing the future risk from heat stress requires considering a portfolio of metrics.

The health risk from heat stress is not spatially homogeneous – neither globally nor within a country or a region – owing to several factors, including variations in local climate conditions, local climate feedbacks (e.g., due to albedo, soil moisture), or differences in the social environment (e.g., population density, socioeconomic conditions). Temperatures are often amplified in cities due to the predominance of impervious surfaces and the multitude of anthropogenic heat sources. The resulting urban heat island (UHI) effect leads to higher levels of ambient heat in cities compared to surrounding areas (e.g., Heaviside et al., 2017). In Europe, our region of study, about 75% of the population lives in urban areas (UN-Habitat, 2011) and the urban population is projected to grow even further in the future along with an ageing trend (Smid et al., 2019). Larger metropolitan areas in Europe will become more vulnerable to extreme heat in the coming decades (Smid et al., 2019) and heat mortality in European cities is projected to significantly increase (Karwat and Franzke, 2021). Cities in Europe or elsewhere are thus becoming climate hotspots in terms of climate change (Zheng et al., 2021) but also for adaptation and innovation (IPCC, 2022)

https://doi.org/10.5194/nhess-2023-99
Preprint. Discussion started: 6 July 2023


Natural Hazards and Earth System Sciences
Discussions

due to the need for adequate strategies to address climate change adaptation. Preventing adverse health outcomes from heat stress and designing appropriate and effective adaptation measures requires accurate projections and estimates of heatwaves and temperature extremes. Recently, climate model simulations have reached a spatial resolution high enough to provide such projections at the city-level.

Analyses of climate and climate change in cities face the challenge of delivering results on spatial resolutions that are high enough to be relevant for cities while robustly estimating the risk of extreme events. Urban models, which can resolve cities at scales of ~100 m or even higher, can deliver great spatial details of cities (e.g., Masson et al., 2020), with the trade-off that often only a limited number of cities are examined (e.g., Goret et al., 2019; Krayenhoff et al., 2020). Analyses with urban models coupled to climate models often rely on data from a single or a few climate models and are thus not able to adequately incorporate climate variability to robustly quantify the probability of extreme events. On the other hand, climate model simulations can be used to quantify climate variability and the risk of extreme events in multiple cities. Guerreiro et al. (2018) used simulations by general circulation models (GCMs) from the Climate Model Intercomparison Project phase 5 (CMIP5) to investigate heatwave projections in European cities. However, GCMs do not fully depict local urban climate conditions as the spatial resolution of GCMs (~100 km) is much coarser than that of urban models and GCMs generally lack a representation of urban areas. To provide higher spatial resolution and to overcome some of the limitations of GCMs, dynamical downscaling by regional climate models is frequently applied. This approach has been used multiple times to investigate individual cities with a single model (e.g., Argueso et al., 2015; Chapman et al., 2019; Keat et al., 2021; Kusaka et al., 2012; Li and Bou-Zeid, 2013; Ramamurthy and Bou-Zeid, 2017; Wouters et al., 2017) but rarely for analysing climate conditions in a large number of cities and/or with an ensemble of models (e.g., Sharma et al., 2019; Smid et al., 2019; Junk et al., 2019). For Europe, an ensemble based on regional climate models (RCMs) from the European branch of the Coordinated Regional Downscaling Experiment (EURO-CORDEX; Jacob et al., 2013; Vautard et al., 2021) is available, providing simulations at a resolution of 0.11° (EUR-11, ~12.5 km), which is fine enough to analyse climate conditions in major European cities at the city-level. The EUR-11 simulations were evaluated by Coppola et al. (2021) and Vautard et al. (2021) who showed that the EURO-CORDEX simulations reproduce well the observed spatial temperature distribution in Europe, despite a general cold bias of summer temperatures of around 1 °C to 2 °C compared to observation-based data from E-OBS (Cornes et al., 2018) in large parts of Europe. Hot biases of extreme temperatures (i.e., hottest five consecutive days) in mountainous regions are reduced in EURO-CORDEX compared to CMIP5, while a cold bias remains in central and northern Europe and a warm bias in southern Europe (Iles et al., 2020). Lin et al. (2022) evaluated the representation of HWMId in a subset of the EURO-CORDEX ensemble against reanalysis data, finding overall good agreement between both datasets and highlighting the added value of RCMs compared to the driving GCMs for representing small-scale features.

EURO-CORDEX simulations have been used to examine how temperatures and ambient heat are projected to increase in the future throughout Europe (Vautard et al., 2013; Molina et al., 2020; Coppola et al., 2021) and for a small group of European cities (Junk et al., 2019; Langendijk et al., 2019; Burgstall et al., 2021), showing that urban areas will be strongly affected by rising temperatures. The different studies used varying sets of metrics, different model ensembles, and different selections of

https://doi.org/10.5194/nhess-2023-99
Preprint. Discussion started: 6 July 2023


Natural Hazards and Earth System Sciences
Discussions

cities. Smid et al. (2019) analysed HWMId projections for European capitals based on eight EURO-CORDEX models at 0.11° resolution, focusing on the metropolitan areas around the capitals. They found highest HWMId increases in southern European cities and, additionally, they highlight that exposure to heatwaves also strongly depends on population density. Junk et al. (2019) analysed projections of several heatwave metrics defined by the Expert Team on Climate Change Detection and Indices (ETCCDI) for London, Luxembourg, and Rome based on 11 EURO-CORDEX models at 0.11° resolution. The considered heatwave metrics project strongest increases for Rome, except for the number of heatwaves per year, which the authors explain by the increasing length of heatwaves, reducing their number. Using wet-bulb globe temperature (WBGT) as a heat metric, Casanueva et al. (2020) analysed exceedances of WBGT thresholds of 26 °C and 28 °C in Europe based on an ensemble of 39 EURO-CORDEX models (using simulations at both 0.11° and 0.44° resolution). Future exceedances of WBGT>28 °C are projected to be highest in southern Europe, followed by central Europe, while exceedance rates are negligible in northern Europe. Based on CMIP5 GCMs, Guerreiro et al. (2018) found that strongest increases in heatwave days are projected for southern European cities along with substantial increases in coastal cities in northern Europe, while maximum temperatures of heatwaves are projected to rise most strongly in central Europe.

Here we build on these studies and use simulations by 72 GCM-RCM model combinations of the 0.11° EURO-CORDEX ensemble to assess projections of ambient heat for 36 major European cities. We focus on near-surface air temperature and compare three metrics: changes in yearly maximum temperature, the number of days per year on which daily maximum temperatures exceed 30 °C, and HWMId. To evaluate potential differences in projections for daytime and nighttime conditions, we additionally consider daily minimum temperature. We first analyse how well the EURO-CORDEX ensemble reproduces the measured temperature distributions in the selected cities compared to reanalysis and observation-based data. Further, we quantify how ambient heat is projected to evolve in these cities under global warming according to the three considered heat metrics. Finally, we evaluate how the choice of metrics affects projections of ambient heat, which can give relevant insights for designing appropriate adaptation measures to counteract health risks from ambient heat. A holistic analysis of the health risk from heat stress comprises the factors heat-related hazards, heat exposure, and vulnerability to heat. We focus on the hazard from extreme heat by employing the three heat metrics, acknowledging that exposure and vulnerability can also vary strongly across cities (Smid et al., 2019; Sera et al., 2019; Gasparrini et al., 2015).

2 Data and Methods

2.1 Data

2.1.1 Cities

We include 36 major European cities in our analysis. These comprise all European cities with a population of more than 1.2 million, and all European capitals with more than 500,000 inhabitants. We register the coordinates and elevation of each city,

https://doi.org/10.5194/nhess-2023-99
Preprint. Discussion started: 6 July 2023

Natural Hazards and Earth System Sciences
Discussions

and whether it is located close to the sea (see Supplementary Table S1). The complete list of cities and their geographic locations are indicated in Figure 1a.

2.1.2 Climate model data

The analysis is based on 72 GCM–RCM model chains from the EURO-CORDEX ensemble, which covers the European domain (Jacob et al., 2013, see Supplementary Table S2 for a detailed list of models). EURO-CORDEX simulations use two different spatial resolutions, 0.11° (EUR-11, ~12.5 km) and 0.44° (EUR-44, ~50 km). We only use data from the higher-resolution EUR-11 simulations, for which typically at least one grid cell falls within the extent of each major European city (Figure 1b). For our analysis, we use daily maximum temperature (tasmax), daily minimum temperature (tasmin), and monthly mean temperature (tas), employing data from historical and RCP8.5 simulations for the period 1981-2100 (note that some model simulations only run until 2099 and one only until 2098). For each city, we use data from the grid cell that is located closest to the centre of each city centre. The large ensemble of 72 GCM–RCM model combinations allows for a robust estimation of future ambient heat including the model structural uncertainty, which has been shown to be relevant for quantifying the risk of urban heatwaves (Zheng et al., 2021). To test the spatial robustness of our results, we additionally consider data from a box of 3x3 grid cells around the city centres.

We further use simulations from the CMIP5 (24 models) and CMIP6 (24 models) ensembles (using one ensemble member per model) for comparison with the EURO-CORDEX simulations (see Supplementary Tables S3 and S4 for a detailed list of the considered CMIP5 and CMIP6 models and ensemble members). We employ data from historical and RCP8.5 simulations (SSP5-8.5 in case of CMIP6), analysing daily maximum temperature (tasmax) and monthly mean temperature (tas) for the same period (1981-2100) as for EURO-CORDEX. Analogous to EURO-CORDEX, we use the grid cell closest to the city centre for our analysis. To evaluate how the downscaling of GCMs by RCMs affects the results, we further consider the CMIP5 model set that is used to drive the 72 EURO-CORDEX RCMs. For this purpose, we create a GCM ensemble, which we denote as “EURO-CORDEX GCM ensemble”, for which we consider each GCM member as many times as it is used as a driving GCM in the EURO-CORDEX ensemble. The EC-EARTH ensemble member r3i1p1 (used to drive several EURO-CORDEX RCMs, see Supplementary Table S2) is not available via the Earth System Grid Federation (ESGF) data portals and we thus substitute it by the EC-EARTH member r1i1p1 to create the EURO-CORDEX GCM ensemble.

https://doi.org/10.5194/nhess-2023-99
Preprint. Discussion started: 6 July 2023

Natural Hazards and Earth System Sciences
Discussions

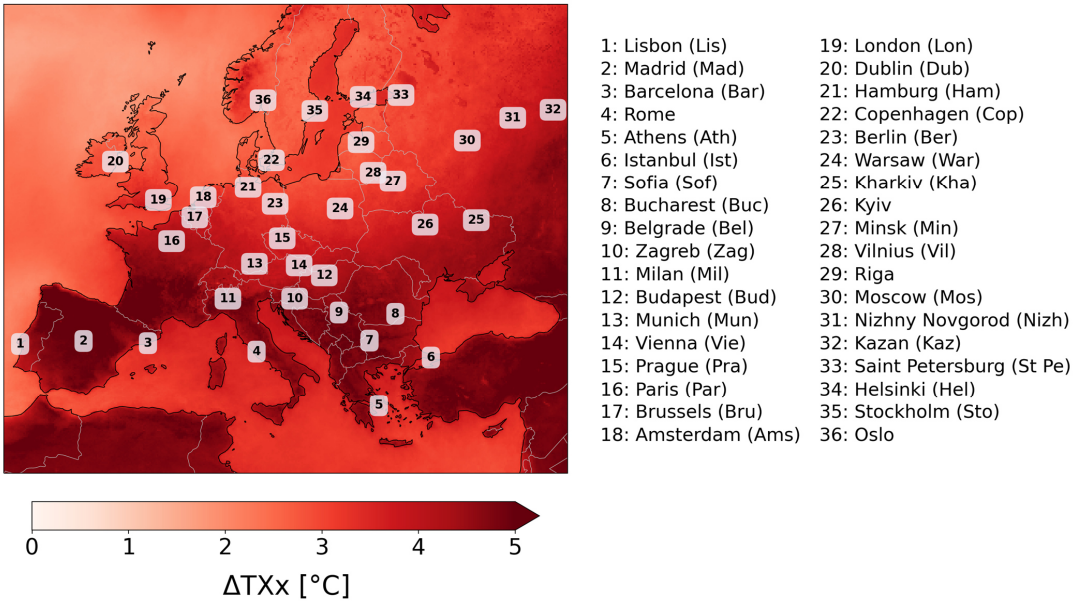

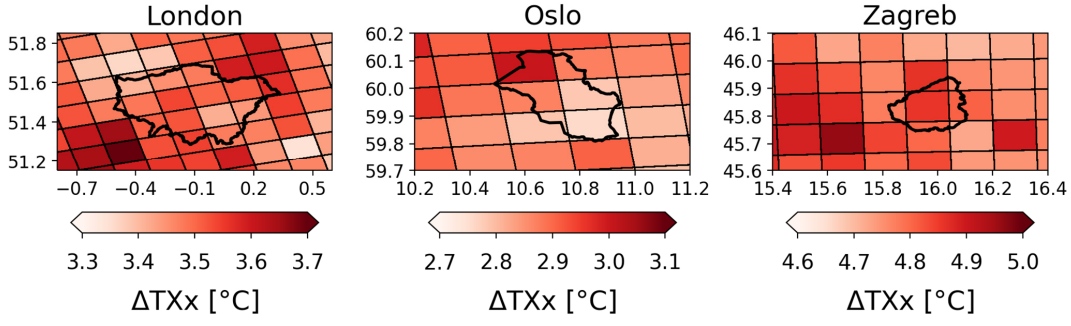

Figure 1: Overview of the cities investigated in this study and examples of the spatial resolution of EURO-CORDEX models. Top: Location of the cities with the background map showing the EURO-CORDEX multi-model median change of annual maximum temperature (ΔTXx) at 3 °C European warming relative to 1981-2010 (see Section 2.2). Abbreviations in the list of cities indicate the abbreviated city names used in Figure 7. Bottom: Example of grid spacing used by the majority of EURO-CORDEX models compared to the extent of three cities with different sizes (black polygons).

https://doi.org/10.5194/nhess-2023-99
Preprint. Discussion started: 6 July 2023


Natural Hazards and Earth System Sciences
Discussions

2.1.3 Reference datasets

We evaluate the EURO-CORDEX simulations (see Section 3.1) by comparing them against two gridded reference datasets: 1) the E-OBS gridded meteorological dataset, which provides gridded meteorological fields interpolated from weather station data at 0.1° resolution for Europe (Cornes et al., 2018) and 2) the global reanalysis ERA5-Land, which provides land variables including 2 m air temperature at a spatial resolution of about 9 km (Muñoz-Sabater et al., 2021). Additionally, we use data from single weather stations that lie within or close to the considered cities, using data from the Global Surface Summary of the Day (GSOD; Smith et al., 2011) and from the European Climate Assessment & Development (ECA&D; Klein Tank et al., 2002; Klok and Klein Tank, 2009). We only include data from weather stations with a data record length of at least 20 years. For all datasets, the evaluation is performed using daily maximum temperatures and daily minimum temperatures in the period 1981-2010. For ERA5-Land, daily maximum and daily minimum temperatures are calculated as maximum and minimum of the hourly 2 m air temperature data. The land scheme of ERA5-Land does not include representations of urban areas. Hence, specific climatic conditions in cities (such as the urban heat island effect, UHI) may not be fully represented. For cities, in which temperature data from weather stations within the city limits are assimilated in ERA5-Land or considered in E-OBS, such effects might, however, be partly included.

2.2 European mean warming

Regional temperatures and temperature extremes scale linearly with global mean surface air temperature (GSAT; Seneviratne et al., 2016; Wartenburger et al., 2017; Seneviratne and Hauser, 2020). Uncertainties connected to the underlying climate scenarios can thus be reduced if expressing future evolutions of regional temperatures as a function of changes in GSAT, usually calculated relative to pre-industrial (1850-1900) conditions. This approach of expressing climate change in terms of global warming levels instead of emission-driven or concentration-driven scenarios has been used by several recent studies (e.g., Schwingshackl et al., 2021; Freychet et al., 2022; Li et al., 2021) and was widely applied in the 6th Assessment Report of the Intergovernmental Panel on Climate Change (IPCC, 2021). While this approach works well on global scales, it cannot be applied directly to the regional climate model simulations of EURO-CORDEX, mainly due to two reasons. First, EURO-CORDEX simulations only start in 1950 (some models in 1970) and pre-industrial reference temperatures are therefore not available. We thus derive changes in mean temperatures relative to the period 1981-2010. Second, the EURO-CORDEX ensemble projects a lower rate of warming in Europe than the CMIP5 ensemble (Coppola et al., 2021). This discrepancy has been attributed to several reasons, such as differences in aerosol forcing (Boé et al., 2020; Gutiérrez et al., 2020; Nabat et al., 2020) or diverging trends in cloudiness (Bartók et al., 2017). To account for this discrepancy, we implement the scaling approach using European mean surface air temperature (ESAT) instead of GSAT based on temperature data from the EURO-CORDEX simulations. We calculate GSAT and ESAT from monthly mean temperature (tas), where ESAT is defined as the average temperature of a box spanning over Europe from 10° W to 35° E and from 30° N to 70° N.

https://doi.org/10.5194/nhess-2023-99
Preprint. Discussion started: 6 July 2023

Natural Hazards and Earth System Sciences
Discussions

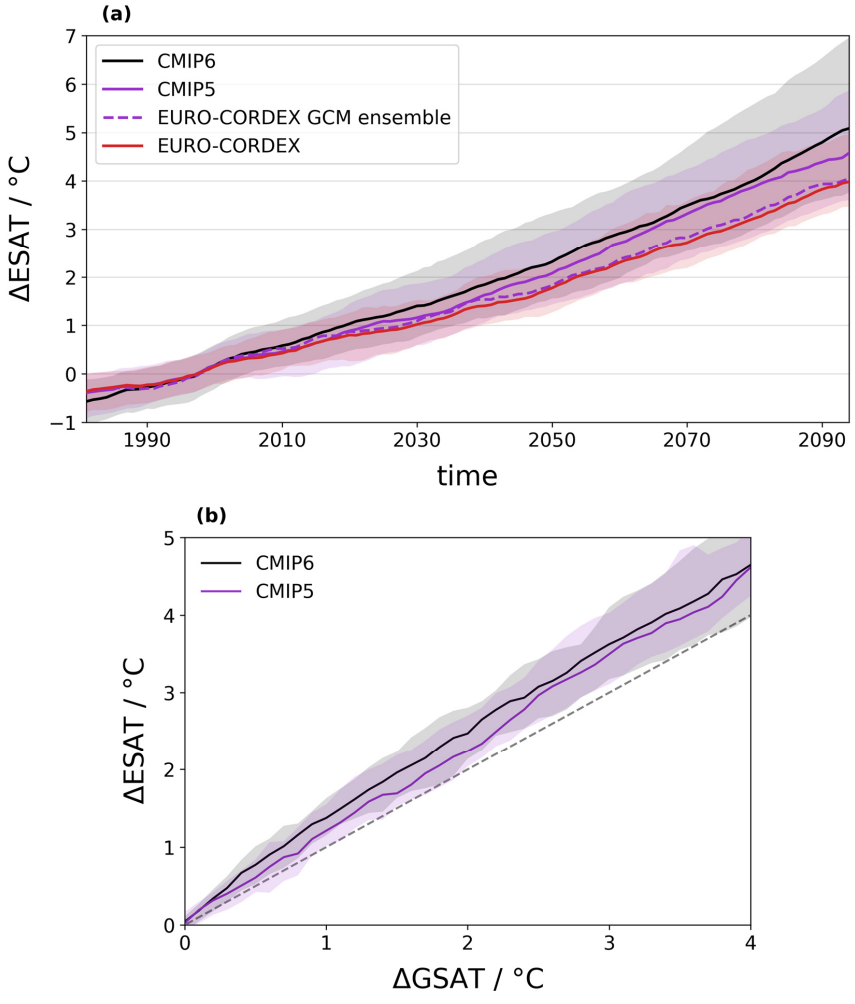

192

193 **Figure 2:** Warming in Europe in the RCP8.5 scenario (EURO-CORDEX, CMIP5) and SSP5-8.5 scenario (CMIP6) relative to
194 1981-2010. (a) Change in European mean surface air temperature (ESAT) as a function of time. The dashed purple line
195 indicates the EURO-CORDEX GCM ensemble (see Section 2.1.2 for more details). (b) Change in ESAT as a function of
196 change in global mean surface air temperature (GSAT) relative to the reference period 1981-2010. Solid lines in (a) and (b)
197 indicate the multi-model median and shading the range from 10th to 90th percentile across models. Data in (a) are smoothed
198 with a 10-year window and data in (b) are interpolated in 0.1 °C steps. The dashed grey line in (b) represents the identity line.

https://doi.org/10.5194/nhess-2023-99
Preprint. Discussion started: 6 July 2023


Natural Hazards and Earth System Sciences
Discussions

Comparing the warming projections in the CMIP5, CMIP6, and EURO-CORDEX ensembles (Figure 2a) confirms that the CMIP5 and CMIP6 ensembles project a faster warming in Europe than the EURO-CORDEX ensemble. However, if considering the EURO-CORDEX GCM ensemble (see Section 2.1.2), the resulting warming projections are very similar to the projections of the EURO-CORDEX ensemble. This indicates a general agreement between the warming projections of CMIP5 and EURO-CORDEX averaged over Europe and suggests that the difference in ESAT is mainly connected to the GCM subset used to drive the EURO-CORDEX RCMs. As ESAT scales well with GSAT (Figure 2b), the warming can also be directly related to changes in GSAT.

For consistency, we choose to stay within the EURO-CORDEX framework and express our results as a function of ESAT instead of GSAT, based on temperature data from the EURO-CORDEX simulations. The results are shown for a European warming of 3 °C relative to 1981-2010. This corresponds to a global warming of 2.5 °C in CMIP5 (2.4 °C to 2.7 °C; interquartile range across models) and of 2.4 °C in CMIP6 (2.3 °C to 2.6 °C) relative to 1981-2010 and to a global warming of around 3.1 °C in CMIP5 (3.0 °C in CMIP6) since pre-industrial conditions (1850-1900). For each GCM–RCM model chain of EURO-CORDEX, we estimate the model-specific time when ESAT increases by 3 °C relative to 1981-2010 using a 20-year window around the first year in which the 20-year average temperature exceeds 3 °C warming. The same approach is applied to CMIP5 and CMIP6 model data.

2.3 Metrics for quantifying ambient heat

Three heat metrics are used in this study to quantify how ambient heat will change in European cities under global warming. The selected metrics were applied in various studies to investigate projections of ambient heat in Europe and globally (e.g., Casanueva et al., 2020; Lin et al., 2022; Coppola et al., 2021; Russo et al., 2015; Dosio et al., 2018). The first metric is the change in yearly maximum temperature (TXx; based on daily maximum temperature data) between the reference period 1981-2010 and the (model-specific) time when European warming reaches 3 °C relative to 1981-2010. The change in TXx indicates how strongly extreme temperatures increase due to climate change.

As a second metric we calculate the number of days per year on which daily maximum temperatures (TX) exceed 30 °C at the time when European warming reaches 3 °C. The threshold of 30 °C is a compromise of being high enough to be relevant for southern European countries and low enough for northern European countries. While absolute thresholds have been used in several scientific studies (e.g., Zhao et al., 2015; Schwingshackl et al., 2021; Casanueva et al., 2020), it should be kept in mind that exceedances of absolute thresholds strongly depend on local climate conditions. To test the sensitivity to the selected threshold level, we investigate how varying the threshold between 25 °C and 33 °C affects the identified geographic patterns. Calculating exceedances of fixed thresholds based on climate model data usually requires bias adjustment to correct for potential model biases (Maraun, 2016). However, we do not apply bias adjustment here due to the lack of reliable reference data, as urban areas are not specifically represented in the reference datasets ERA5-Land and E-OBS. Consequently, the urban heat island effect might be underrepresented in these datasets. Instead, we test the effect of bias adjustment by applying a simple correction that 1) adjusts the mean of the climate model data to ERA5-Land, and 2) adjusts the mean and variability to

https://doi.org/10.5194/nhess-2023-99
Preprint. Discussion started: 6 July 2023

ERA5-Land (i.e., by applying a transformation to standard score). For this purpose, the mean and standard deviation of daily maximum and daily minimum temperatures in summer (June, July, August) is calculated for each grid cell in a box of 5x5 grid cells around the centre of each city in the reference period 1981-2010. The resulting values are averaged over the 5x5 box and used for bias adjustment. The 5x5 box is used to represent the climate conditions within and around each city. The ERA5-Land data is bilinearly interpolated to the grid of each EURO-CORDEX model before calculating the mean and standard deviation. We use a Kolmogorov-Smirnow test to check whether the bias-adjusted heat metrics are statistically significantly different from the heat metrics calculated from the original data.

The third metric that we apply is the Heat Wave Magnitude Index daily (HWMId, Russo et al., 2015), which integrates both the length and the magnitude of a heatwave to calculate its overall strength. In the context of HWMId, heatwaves are defined as at least three consecutive days with daily maximum temperatures above the 90th percentile of the daily maximum temperature distribution of all days within a 31-day window in a pre-defined reference period (Russo et al., 2015). For each day in a heatwave, the HW magnitude (HW_M) is calculated by subtracting the 25th percentile of TXx in the reference period 1981-2010 from daily maximum temperature (TX), normalised by the interquartile range of TXx in the reference period:

$$HW_M = \begin{cases} \frac{TX - TXx_{25p}}{TXx_{75p} - TXx_{25p}}, & \text{if } TX > TXx_{25p} \\ 0, & \text{otherwise} \end{cases} \quad (1)$$

The sum over all daily HW magnitudes of a heatwave yields HWMId. By definition, HWMId takes into account the interannual temperature variability of each location. We calculate HWMId using daily maximum temperature (denoted as HWMId-TX) for the time when European warming reaches 3 °C with 1981-2010 as the reference period. In each year, we identify the heatwave with the highest HWMId-TX and use it to calculate the 20-year average HWMId-TX.

To represent nighttime conditions, we further calculate the three different metrics based on daily minimum temperature (TN), i.e., the yearly maximum of daily minimum temperatures (TNx), the number of tropical nights (TN>20 °C), and HWMId based on daily minimum temperatures (HWMId-TN).

2.4 Statistical analysis

2.4.1 Spatial patterns of ambient heat

To analyse how a city's geographic location and local climate affect projections of ambient heat according to the three metrics, we estimate the contribution of different factors for explaining the spatial pattern of ambient heat across European cities. We separately analyse the spatial correlation of each heat metric with four climatological factors (summer mean daily maximum temperature $\underline{TX}_{ref}$ and its standard deviation $\sigma_{TX,ref}$ in the reference period; change in summer mean daily maximum temperature $\Delta\underline{TX}$ and change in its standard deviation $\Delta\sigma_{TX}$ between reference and application periods) and four location

https://doi.org/10.5194/nhess-2023-99
Preprint. Discussion started: 6 July 2023

factors (latitude, longitude, elevation, flag indicating whether a city is located close to the sea). Summer is defined as the months June, July, and August.

The explanatory variables (i.e., climatological or location factors) may be correlated, and their contributions cannot be strictly disentangled. We therefore use an approach based on semipartial correlation to quantify the average contribution of each variable to the total explained variance R^2 (Schwingshackl et al., 2018). The squared semipartial correlation measures how much of the remaining unexplained variance is explained by an explanatory variable that is introduced after several others have already been considered. If explanatory variables are independent, the sum of the squared semipartial correlation coefficients yields R^2. For correlated explanatory variables, the additional contribution of an explanatory variable can be estimated by the average R^2 increase of adding the variable to all regression models that contain a subset of the other explanatory variables (Azen and Budescu, 2003; Schwingshackl et al., 2018). If using the averaging method proposed by Azen and Budescu (2003), the sum of all squared semipartial correlations is equal to R^2. The variability of the squared semipartial correlation estimates is a measure for collinearities between the explanatory variables and can be used as an uncertainty estimate for the contribution of each explanatory variable.

2.4.2 Relative importance of RCMs and GCMs

We further quantify how much of the variability in ambient heat across the EURO-CORDEX ensemble is due to the choice of GCMs or RCM, respectively. We follow the variance decomposition method of Sunyer et al. (2015) to calculate the variance due to RCMs, due to GCMs, and due to the interaction between RCMs and GCMs. As the interaction term cannot be attributed to either GCMs or RCMs, we interpret it as uncertainty and indicate the contribution of RCMs and GCMs as a range that once includes and once excludes the contribution of the interaction term. For each heat metric, we calculate the percentage contribution of RCMs and GCMs to the total variance across all 72 RCM-GCM model chains.

3 Results

3.1 Evaluation of EURO-CORDEX ensemble

To evaluate how well the EURO-CORDEX models reproduce observed temperatures in the 36 major European cities, we compare their temperature distribution to data from E-OBS, ERA5-Land, and weather stations. Figure 3 shows the distributions of summer mean daily maximum temperatures in 1981-2010 for all cities as a function of distance from the city centre. Detailed bias distributions for all cities can be found in Supplementary Figure S1. The distribution of the EURO-CORDEX models generally matches the reference data well but is often wider than the distributions of the reference datasets (Figure 3). The EURO-CORDEX simulations reveal a cold bias in many cities lying in the northern and eastern parts of Europe (Dublin, Helsinki, Kazan, Nizhny Novgorod, Oslo, Saint Petersburg, Stockholm), ranging from -1.3 °C to -2.7 °C relative to E-OBS and from -0.3 °C to -1.2 °C relative to ERA5-Land. A warm bias – particularly relative to ERA5-Land – is found for several cities in south-eastern Europe (Belgrade, Bucharest, Kharkiv, Kyiv), ranging from +0.2 °C to +1.0 °C relative to E-OBS and

https://doi.org/10.5194/nhess-2023-99
Preprint. Discussion started: 6 July 2023

from +1.7 °C to +3.2 °C relative to ERA5-Land. ERA5-Land and E-OBS also show systematic differences, with daily maximum temperatures in ERA5-Land being mostly colder than E-OBS and the weather station data. Consequently, the magnitude and sign of the EURO-CORDEX biases strongly depend on the reference dataset. The multi-model median of the EURO-CORDEX ensemble has a warm bias relative to ERA5-Land (+0.5 °C on average across cities) and a cold bias relative to E-OBS (-0.8 °C on average), which is consistent with the findings of Vautard et al. (2021).

The distributions of daily minimum temperatures in the EURO-CORDEX models also generally match the reference datasets (Supplementary Figure S2), but in several cities biases are more pronounced than for maximum temperatures. The EURO-CORDEX ensemble has a cold bias relative to E-OBS (-0.6 °C on average; most pronounced in Saint Petersburg, Nizhny Novgorod, Copenhagen, Lisbon, Madrid) and to ERA5-Land (-0.8 °C on average; most pronounced in Kazan, Helsinki, Istanbul, Riga, Stockholm). In contrast to the lower daily maximum temperature values in ERA5-Land, daily minimum temperatures in ERA5-Land are warmer than E-OBS in several of the investigated cities.

In several cities, temperatures change depending on the distance from the city centre (Figure 3, Supplementary Figure S2). E-OBS shows higher temperatures close to the city centre in Budapest, Prague, and Vienna, while for EURO-CORDEX this is the case in Athens, Brussels, Dublin, Minsk, Munich, Paris, Rome, and Vienna. Yet, these temperature gradients are not necessarily due to UHI but could also be caused by other factors, such as gradients in elevation. For E-OBS and the weather station data, the scarce station density close to the city centres as well as the standard conditions for meteorological measurements (i.e., measurements are taken over grasslands) might be reasons for the lack of pronounced UHI effects. For the other datasets, this might be due to the missing representation of urban areas in the land surface schemes of ERA5-Land and in many of the EURO-CORDEX models.

https://doi.org/10.5194/nhess-2023-99
Preprint. Discussion started: 6 July 2023

Natural Hazards and Earth System Sciences
Discussions
Open Access
EGU

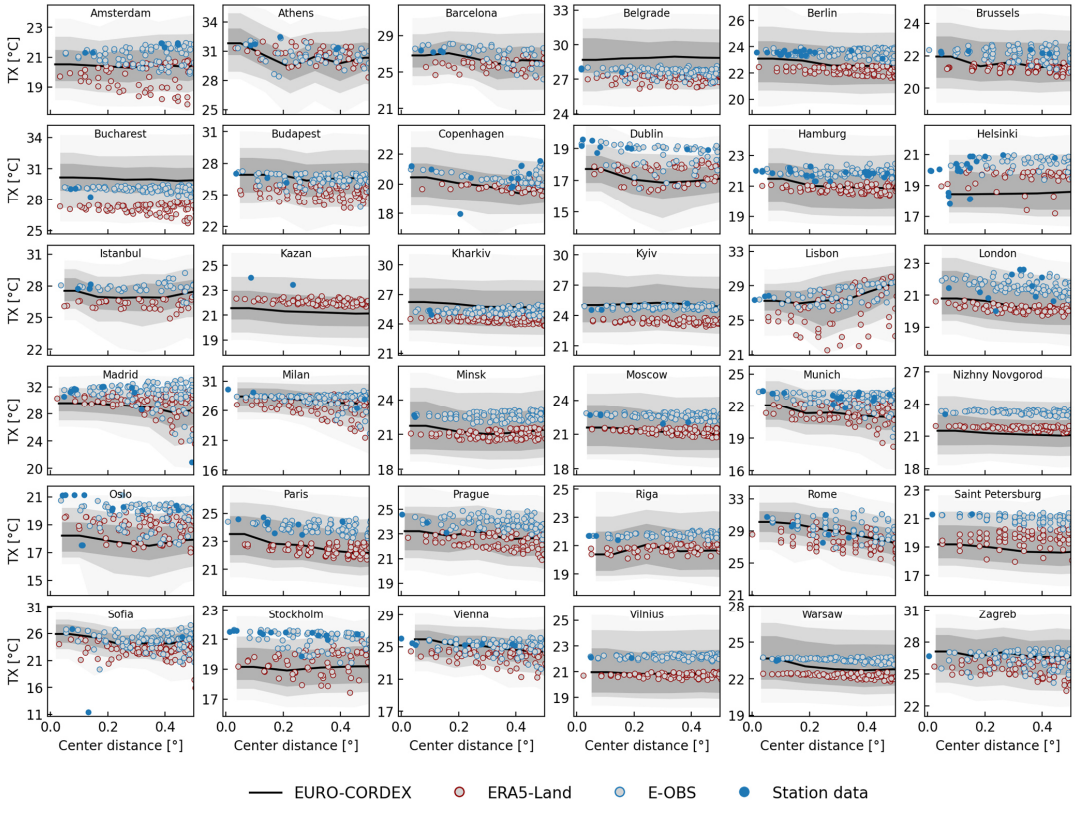

Figure 3: Distribution of daily maximum temperature (TX) in summer for the investigated European cities as function of distance to the city centre. The plot shows summer (June, July, August) average TX over the period 1981-2010 for EURO-CORDEX (black line and grey shading), ERA5-Land (red-edged grey dots), E-OBS (blue-edged grey dots), and station data (filled blue dots). The black line for EURO-CORDEX denotes the multi-model median, dark grey shading the interquartile range across models, and light (very light) grey shading the range from 10th (1st) to 90th (99th) percentile. Only temperatures on land are included (sea areas are masked).

https://doi.org/10.5194/nhess-2023-99
Preprint. Discussion started: 6 July 2023

3.2 Projections of ambient heat for major European cities

The EURO-CORDEX projections for major European cities show increasing ambient heat under 3 °C European warming with distinct geographical patterns for the three different metrics (Figure 4). Increases in TXx are largest in southern Europe, followed by western and eastern Europe, and lower towards northern Europe. The top five cities in terms of TXx increase (Milan, Madrid, Sofia, Zagreb, Belgrade; numbered from 1 to 5 in Figure 4) are all located in southern Europe but none of them is located directly close to the sea. Cities in southern Europe located at or close to the sea (e.g., Lisbon, Barcelona, Rome, Athens, Istanbul) also show substantial TXx increase, yet weaker than the cities situated more inland.

The yearly number of days on which TX exceeds 30 °C shows a clear south-north gradient, with values being highest in Athens, Madrid, Rome, Bucharest, and Milan (numbered 1 to 5). These cities exceed 30 °C on more than 80 d/y, while the five cities with lowest exceedance rates (all lying in northern Europe; numbered 32 to 36) experience on average less than 2 d/y above 30 °C. Additionally, local climate conditions can play an important role as well, for example in the case of Barcelona, Istanbul, and Sofia, which have lower exceedance rates than the surrounding cities. Varying the threshold level between 25 °C and 33 °C considerably changes the number of yearly exceedance days, but the geographical distribution is not altered much (Supplementary Figure S3).

HWMId-TX is largest in southern European cities, followed by eastern European cities, with values being highest in Barcelona, Madrid, Milan, Sofia, and Rome (numbered 1 to 5). In contrast to the other two metrics, cities located in northern Europe also show high HWMId-TX values (e.g., Oslo, Copenhagen, Stockholm, Helsinki), while lowest HWMId-TX values are projected in an arc spanning from the Netherlands over northern Germany towards the Baltic states.

Several cities show high levels of ambient heat for all investigated heat metrics (e.g., Athens, Belgrade, Bucharest, Madrid, Milan, Sofia, Zagreb), while other cities reveal a strong dependency on the metric under consideration. Barcelona, for example, ranks number one in terms of HWMId-TX, but exceeds 30 °C only rarely. Lisbon has substantial increases in TXx and temperatures often exceed 30 °C, but HWMId-TX is rather low. Kazan has substantial increases in TXx and high HWMId-TX values, but TX exceedances above 30 °C are relatively low. Oslo ranks among the cities with weakest changes in TXx and with lowest TX exceedances above 30 °C, but with high HWMId-TX values. Considering only one metric might thus lead to unbalanced conclusions about projections of ambient heat for urban areas, potentially underestimating future risks from heat stress.

https://doi.org/10.5194/nhess-2023-99
Preprint. Discussion started: 6 July 2023

Natural Hazards and Earth System Sciences
Discussions

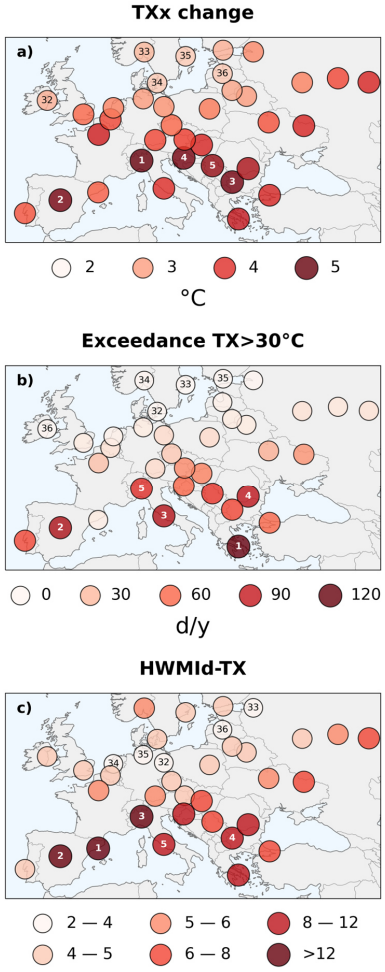

Figure 4: Projections of ambient heat at 3 °C European warming according to three different heat metrics for 36 major European cities as simulated by the EURO-CORDEX ensemble. a) Change in yearly maximum temperature (TXx) between 1981-2010 and 3 °C European warming, b) TX exceedances above 30 °C at 3 °C European warming, and c) Heat Wave Magnitude Index daily based on TX (HWMId-TX) at 3 °C European warming. The values indicate the multi-model median of the EURO-CORDEX ensemble. Numbers in the circles from 1 to 5 (32 to 36) indicate the five cities with highest (lowest) ambient heat according to each metric.

https://doi.org/10.5194/nhess-2023-99
Preprint. Discussion started: 6 July 2023

3.3 Identifying factors influencing the spatial patterns of ambient heat across cities

To better understand the projected spatial patterns of the three heat metrics, we estimate how much of the spatial variance is explained by different climate factors, representing each city's temperature climatology as well as its projected changes, and location factors (Figure 5). Generally, the considered climate factors ($\overline{TX}_{ref}$, $\sigma_{TX,ref}$, $\Delta\overline{TX}$, and $\Delta\sigma_{TX}$; see Section 2.4 for their definition) explain more of the spatial patterns than the location factors (latitude, longitude, elevation, location close to sea). Regarding climate factors (Figure 5a), the spatial pattern of TXx change is mostly influenced by the climate factors $\Delta\overline{TX}$ and $\Delta\sigma_{TX}$, while climate conditions in the reference period do not contribute significantly. For TX exceedances above 30 °C, the maximum temperature in the reference period contributes by far the most, followed by $\Delta\overline{TX}$. For HWMId-TX, the strongest contributions stem from $\Delta\overline{TX}$ and $\sigma_{TX,ref}$. Regarding location factors (Figure 5b), latitude, longitude, and whether a city is located close to the sea partly explain the spatial pattern of TXx change, albeit with rather low model agreement. For the TX exceedances above 30 °C, latitude plays the dominant role, while the contributions of all other factors remain negligible. For HWMId-TX, the explanatory power of all location factors remains low, with latitude being the only factor that explains some of the signal.

Across the three metrics, most of the spatial variability can be explained for the TX exceedances above 30 °C (R^2=0.78 for climate and R^2=0.59 for location factors; considering only variables with significant contribution in at least 50% of the EURO-CORDEX models), followed by TXx change (R^2=0.58 for climate and R^2=0.50 for location factors), while the explained variance of the spatial patterns of HMWId remains rather low (R^2=0.42 for climate and R^2=0.19 for location factors). The contribution of the single climate factors depends strongly on the selected metric, whereas for location factors only latitude plays a major role. All other location factors – despite being statistically significant in some cases – only contribute little to the total variance explained. The high uncertainty for the contribution of some explanatory variables (e.g., $\Delta\overline{TX}$ and $\Delta\sigma_{TX}$ for TXx change, $\overline{TX}_{ref}$ and $\Delta\overline{TX}$ for TX exceedances above 30 °C) points to collinearities between these explanatory variables, which can, however, not be disentangled based on correlation analysis.

https://doi.org/10.5194/nhess-2023-99
Preprint. Discussion started: 6 July 2023

Natural Hazards and Earth System Sciences
Discussions
Open Access
EGU

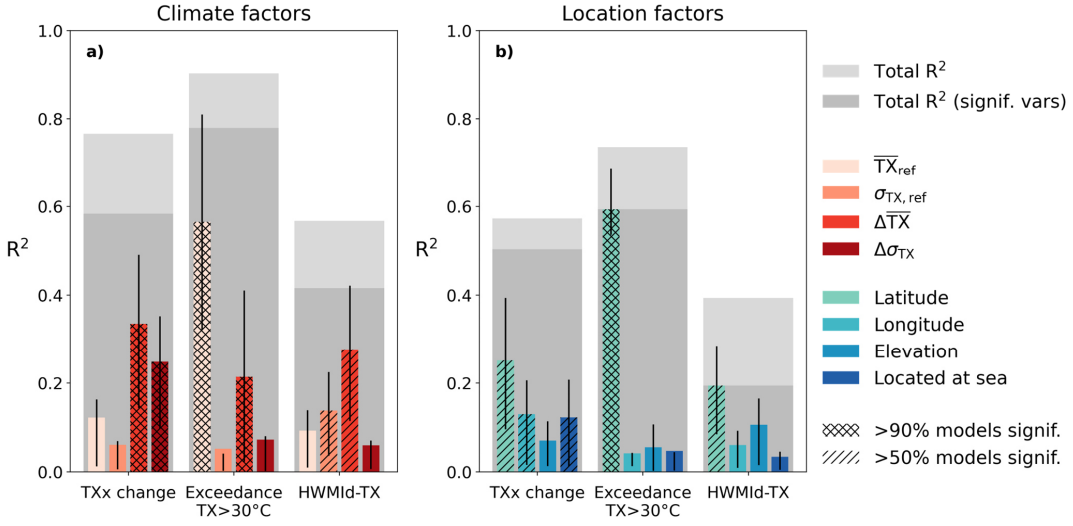

Figure 5: Contribution of different explanatory variables to the explained variance (R^2) of the spatial patterns of ambient heat across European cities in the EURO-CORDEX ensemble. Explanatory variables are divided into a) climate factors (summer mean daily maximum temperature $\overline{TX}_{ref}$ and its standard deviation $\sigma_{TX,ref}$ in the reference period; change in summer mean daily maximum temperature $\Delta\overline{TX}$ and its standard deviation $\Delta\sigma_{TX}$ between the reference period 1981-2010 and 3 °C European warming) and b) location factors. Coloured bars denote the median estimate for each factor, black whiskers denote the uncertainty indicated as interquartile range (calculated from the pooled data of all 72 EURO-CORDEX models and eight regression models). Hatching with lines (crosses) indicates whether at least 50% (90%) of the EURO-CODEX models indicate statistically significant contribution of the respective explanatory variable (Student's t-test, $p<0.05$). Background bars coloured in light grey indicate total R^2 considering all explanatory variables, background bars in dark grey indicate total R^2 if considering only explanatory variables that are statistically significant in at least 50% of the EURO-CORDEX models (Student's t-test, $p<0.05$). The contribution of each climate/location factor is estimated by semipartial correlation (see Section 2.4).

https://doi.org/10.5194/nhess-2023-99
Preprint. Discussion started: 6 July 2023

3.4 Comparing projections of ambient heat during daytime and nighttime

The results presented so far are based on daily maximum temperature and are thus mostly indicative for daytime conditions. We additionally consider daily minimum temperature (TN) to investigate projections of ambient heat during nighttime, which play an important role for human health as well, since elevated nighttime temperatures can reduce people's capacity to recover and thus weaken their physical conditions (Royé et al., 2021; Thompson et al., 2022). The geographical patterns of the TN-based heat metrics are generally similar to the TX-based patterns (Figure 6) with highest levels of ambient heat in southern European cities. Yet, several distinct differences are evident. The TNx increase is generally smaller than the TXx increase, except for cities located at the Baltic Sea, which exhibit a stronger increase in TNx than TXx. Days with TN>20 °C ("tropical nights") are rarer than days with TX>30 °C, except for Barcelona and Istanbul, both of which having substantially more days with TN>20 °C than TX>30 °C (note that no bias adjustment was applied neither for TN>20 °C nor for TX>30 °C; bias-adjusting the mean of the TN distribution based on ERA5-land data even increases the days with TN>20 °C in Barcelona and Istanbul; not shown). In northern Europe, days with TN>20 °C or TX>30 °C both occur very rarely, and differences are thus negligible. Varying the TN threshold level between 15 °C and 23 °C considerably changes the number of yearly exceedance days, but the geographical distribution is not altered much (not shown). HWMId-TN shows much higher values than HWMId-TX, particularly in southern European cities but also in central European cities and in several cities located at the Baltic Sea. Differences between HWMId-TN and HWMId-TX are particularly large in Istanbul, Barcelona, and Rome. The higher HWMId-TN values suggest that nighttime heatwaves will become more severe than daytime heatwaves in the investigated cities as compared to the typical nighttime and daytime climate conditions of the recent past (1981-2010).

https://doi.org/10.5194/nhess-2023-99
Preprint. Discussion started: 6 July 2023

Natural Hazards and Earth System Sciences
Discussions

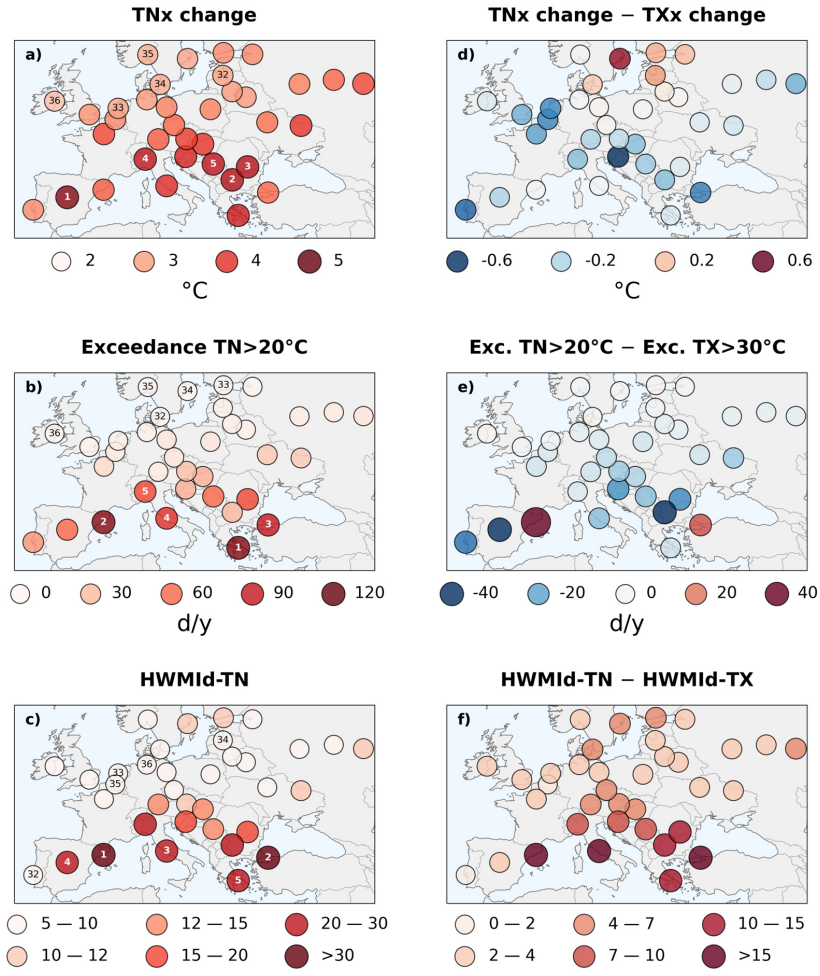

Figure 6: As in Figure 4 but for daily minimum temperature (TN) in panels (a) - (c). Panels (d) - (f) show the difference between ambient heat estimates based on TN and based on daily maximum temperature (TX). Note that the scale for HWMId-TN differs from the HWMId-TX scale in Figure 4.

https://doi.org/10.5194/nhess-2023-99
Preprint. Discussion started: 6 July 2023

3.5 EURO-CORDEX projections of ambient heat in comparison to CMIP5 and CMIP6 projections

We further compare the projections of ambient heat by the EURO-CORDEX, CMIP5, and CMIP6 ensembles for the 36 European cities (Figure 7). The general patterns of CMIP5 and CMIP6 reflect the results of Figure 4, showing a strong TXx increase in south-eastern and eastern European cities, high TX exceedance rates of 30 °C in southern and some eastern European cities, and high HWMId-TX values in southern and some northern European cities (note the logarithmic axis for the latter). In terms of TXx change, the CMIP5 and CMIP6 ensembles generally project a stronger increase in ambient heat than the EURO-CORDEX models, particularly in south-eastern, eastern, and north-eastern European cities, while, for Lisbon, Athens, and Istanbul, the EURO-CORDEX ensemble projects stronger TXx increases. Regarding TX exceedances above 30 °C, the EURO-CORDEX ensemble projects much higher exceedance rates than the CMIP5 and CMIP6 ensembles in southern European cities (e.g., Lisbon, Milan, Athens, Istanbul), whereas the CMIP5 and CMIP6 ensembles show larger exceedance rates in north-eastern European cities and in Barcelona. The CMIP5 and CMIP6 ensembles project higher HWMId-TX values in almost all cities except Madrid, Nizhny Novgorod, and Kazan. Differences in HWMId-TX between the CMIP5 and CMIP6 and EURO-CORDEX ensembles are particularly pronounced in Stockholm, Rome, Athens, and Istanbul. The projected geographical patterns of ambient heat from the CMIP5 and CMIP6 ensembles are generally similar; notable differences are only found for TX exceedances above 30 °C, where CMIP6 has substantially higher values in southern European cities and CMIP5 in northern European cities.

To investigate the effect of dynamical downscaling by RCMs, we additionally consider the projections of ambient heat by the EURO-CORDEX GCM ensemble (dashed purple line in Figure 7; see Section 2.1.2 for its definition). The EURO-CORDEX GCM ensemble resembles more closely the results of the CMIP5 ensemble than of the EURO-CORDEX ensemble, except for some cities (e.g., Amsterdam, Copenhagen, Stockholm, Saint Petersburg, Nizhny Novgorod for TXx changes; Rome for TX exceedances above 30 °C; Lisbon for HWMId-TX). In combination with the fact that the EURO-CORDEX GCM ensemble shows show very similar ESAT trends to the EURO-CORDEX RCM ensemble (Figure 2a), this indicates that differences in projections of ambient heat between the EURO-CORDEX and CMIP5 ensembles are mostly connected to the dynamical downscaling by RCMs. For cities located close to mountains (e.g., Athens) or close to the sea (e.g., Lisbon, Barcelona, Stockholm), the higher spatial resolution of RCMs should thus deliver more accurate estimates than the more coarsely resolved GCMs. This is reflected in the large differences between CMIP5 and EURO-CORDEX estimates for several cities, particularly for TX exceedances above 30 °C and for HWMId-TX.

https://doi.org/10.5194/nhess-2023-99
Preprint. Discussion started: 6 July 2023

Natural Hazards and Earth System Sciences
Discussions

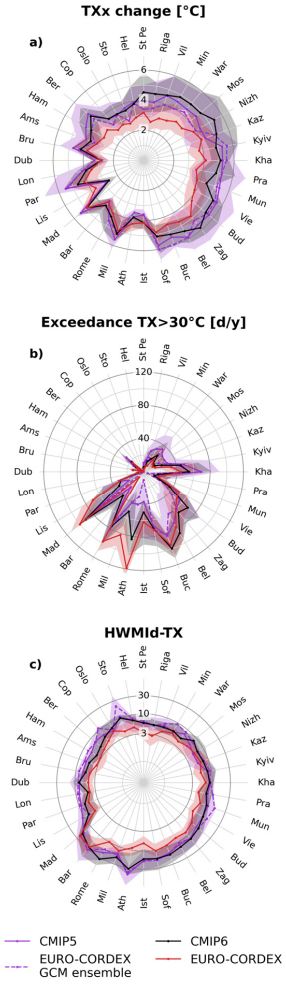

Figure 7: Projections of ambient heat in European cities for EURO-CORDEX, CMIP5, CMIP6, and the EURO-CORDEX GCM ensemble. Cities are arranged according to their geographical location, i.e., northern European cities at the top, eastern European cities on the right, southern European cities at the bottom, and western European cities on the left. a) Change in yearly maximum temperature (TXx) between 1981-2010 and 3 °C European warming, b) TX exceedances above 30 °C at 3 °C European warming, c) Heat Wave Magnitude Index daily based on TX (HWMId-TX) at 3 °C European warming. Note the logarithmic axis for the HWMId-TX panel. Lines indicate the multi-model median and shading the interquartile range across models.

https://doi.org/10.5194/nhess-2023-99
Preprint. Discussion started: 6 July 2023

Natural Hazards and Earth System Sciences
Discussions

3.6 Uncertainty of ambient heat projections

To evaluate the robustness of our results, we estimate how strongly the estimates of ambient heat vary across the EURO-CORDEX models and how much they change in space, that is, within a box of 3x3 grid cells around the grid box located closest to the city centres. The large ensemble of 72 GCM-RCM combinations enables a thorough assessment of the model uncertainty, which we quantify here as the interquartile range (IQR) across models (Figure 7). Uncertainties of TXx change lie between 1 °C and 2 °C in almost all cities, with uncertainties being lowest in southern European cities (where uncertainties are ~1 °C). For TX exceedances above 30 °C, we calculate relative uncertainties (IQR divided by multi-model median; not shown) to reflect the large variability of exceedance rates across cities. The relative uncertainties of TX exceedances above 30 °C are lowest in southern European cities (between 20% and 60%) except for Barcelona, where the relative uncertainty is larger than 300% (and the distribution is skewed towards higher values). In contrast to the other metrics, the uncertainties of HWMId-TX are higher in southern European cities (uncertainties lying between 4 and 8) than in northern European cities (uncertainties lying between 2 and 6), with uncertainties being highest in Barcelona (IQR = 32) followed by Madrid (IQR = 13).

To quantify the spatial variability of ambient heat, heat metrics are calculated individually for each grid cell in a box of 3x3 grid cells around the city centres. The spatial variability is quantified by how much ambient heat varies over the 3x3 grid cells (Supplementary Figure S4). In the large majority of cities, the TXx change estimates remain very similar if using the 3x3 box, indicating that the estimated trends in TXx do not change much within the grid cells surrounding the city centres. Lisbon, Barcelona, Athens, Helsinki, and Istanbul are the cities with the largest spatial variability in TXx changes. Regarding TX exceedances above 30 °C, the largest variabilities are found in Lisbon, Barcelona, Athens, Istanbul, Rome, and Sofia. HWMId-TX values show very large spatial variability in Barcelona and Helsinki, and pronounced variability in Istanbul, Copenhagen, Athens, and Dublin. If only considering grid cells with land fractions larger than 25%, 50%, or 75%, the variability decreases substantially in almost all the cities with large spatial variability in heat metrics. This suggests that ambient heat strongly differs between land and sea areas, particularly for HWMId-TX and for TX exceedances above 30 °C. For HWMId-TX this might be due to the higher TXx variability over land areas than over the sea in the reference period 1981-2010 (Supplementary Figure S5), resulting in much larger HWMId-TX values over sea than over land. Consequently, cities located close to the sea might be affected by this stark land-sea contrast, particularly if their climate is strongly influenced by the sea.

We further test how TX exceedances above 30 °C in the grid cell closest to the centre of each city change if applying a simple bias adjustment method that 1) adjusts the mean of each EURO-CORDEX model to the mean of the ERA5-Land data and 2) adjusts both the mean and the standard deviation (Supplementary Figure S6, see also Section 2.3 for methodological details). The most striking effect of bias-adjusting the data is a reduced uncertainty of the projected TX exceedances above 30 °C. Moreover, the bias-adjusted exceedance rates are statistically significantly lower in 13 cities and higher in 2 cities if only the mean is adjusted (Kolmogorov-Smirnow test, $p<0.05$); and lower in 15 cities and higher in 6 cities if both mean and standard deviation are adjusted. In the remaining cities, the differences are not statistically significant. The effects of bias adjustment

https://doi.org/10.5194/nhess-2023-99
Preprint. Discussion started: 6 July 2023

Natural Hazards and Earth System Sciences
Discussions

are largest in Lisbon, Rome, Sofia, and Bucharest with substantially lower exceedance rates in case of bias adjustment. Adjusting only the mean or adjusting both mean and standard deviation generally yields similar results (differences are largest in Istanbul and Lisbon) with the latter method tending to yield lower exceedance rates.

The rather complete matrix of RCM-GCM combinations enables us to quantify how much of the variability in ambient heat across the EURO-CORDEX models is due to the choice of GCMs or RCMs (Figure 8, see section 2.4.2 for methodological details). The variability across all RCM-GCM combinations is mostly due to RCMs (60% to 75% for TXx change, 60% to 70% for TX exceedances above 30 °C, and 50% to 65% for HWMId-TX), highlighting that the downscaling by RCMs plays a crucial role for the ambient heat estimates in urban areas. Additionally, several patterns can be identified for certain RCMs and GCMs, which indicates that the choice of RCMs and GCMs is also important. Among RCMs, projections of ambient heat in terms of TXx change and HWMId-TX are highest for HadREM3-GA7-05, and in terms of TX exceedances above 30 °C values are highest for WRF381P, HadREM3-GA7-05, and ALADIN63. Comparatively low increases in ambient heat are projected by the RCMs HIRHAM5, RACMO22E, and COSMO-crCLIM-v1-1. Differences between GCMs are less pronounced. Projections of ambient heat are highest for NorESM1-M and CanESM2 in terms of TXx change, for CanESM2, HadGEM2-ES, and MIROC5 in terms of TX exceedances above 30 °C, and for NorESM1-M, CanESM2, and MIROC5 in terms of HWMId-TX. It should be noted though that the results for CanESM2 and MIROC5 might be less robust as each of them is only used twice as driving GCM. Comparatively low increases in ambient heat are projected by CNRM-CM5 and IPSL-CM5A-MR for TXx change, by EC-EARTH and CNRM-CM5 for TX exceedances above 30 °C, and by CNRM-CM5 and MPI-ESM-LR for HWMId-TX.

https://doi.org/10.5194/nhess-2023-99
Preprint. Discussion started: 6 July 2023

Natural Hazards and Earth System Sciences
Discussions
Open Access
EGU

500

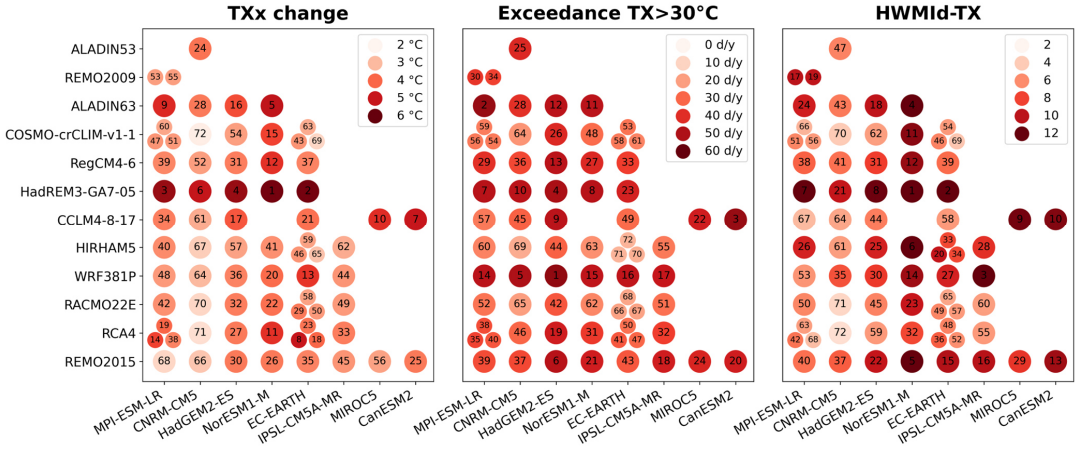

501

502 **Figure 8:** GCM-RCM matrix of EURO-CORDEX models for the change in yearly maximum temperature (TXx) between
503 1981-2010 and 3 °C European warming, b) TX exceedances above 30 °C at 3 °C European warming, c) Heat Wave Magnitude
504 Index daily based on TX (HWMId-TX) at 3 °C European warming. Each circle indicates the average value across all
505 investigated cities for each individual EURO-CORDEX model. Numbers in the circle indicate the ranking of models from 1
506 (highest ambient heat) to 72 (lowest ambient heat). Multiple ensemble members for a GCM-RCM combination are indicated
507 as smaller circles.

https://doi.org/10.5194/nhess-2023-99
Preprint. Discussion started: 6 July 2023


Natural Hazards and Earth System Sciences
Discussions

4 Discussion

4.1 Interpretation and implications of results

All three analysed heat metrics show strong increases in ambient heat in southern European cities at 3 °C European warming. Substantial increases in ambient heat are also evident in other European regions; yet, the spatial patterns strongly depend on the metric under consideration. TXx increases considerably in western and eastern Europe, TX exceedances above 30 °C show a clear south-north gradient with almost no exceedances in northern European cities, and HWMId-TX yields comparatively high values in eastern and northern European cities. This has implications for the estimation of future heat stress, as the projected outcomes can vary strongly depending on the considered metric. For instance, regions in northern Europe that are usually not considered as very prone to heat stress show relatively high values of HWMId-TX. Since health impacts do not only depend on universal physiological limits but also on the climate conditions people are used to (Petkova et al., 2014; Åström et al., 2013), metrics considering the climatology of a region (such as HWMId-TX) can give important insights into the risk of future heat stress that might otherwise be missed. This also concerns nighttime conditions, as HWMId-TN is even higher than HWMId-TX (Figure 6).

The identified spatial patterns broadly agree with results of other studies, showing an increase in heatwave risk in southern Europe along with substantial increases in coastal regions in northern Europe (Guerreiro et al., 2018; Smid et al., 2019; Lin et al., 2022) – as we find for HWMId-TX – and a clear south-north gradient in exceedances of WBGT>28 °C (Casanueva et al., 2020) – consistent with the patterns of TX exceedances above 30 °C. Guerreiro et al. (2018) found that temperatures during heatwaves increase strongest in central Europe, while the TXx increases estimated in our study are highest in southern European cities. This discrepancy between the findings of Guerreiro et al. (2018) and our results could, on the one hand, be related to the fact that TXx does not directly reflect temperatures during heatwaves. On the other hand, it could also be due to the more pronounced increase of extreme temperatures in central Europe in CMIP5 compared to EURO-CORDEX (Supplementary Figure S7).

In some cities, the ranking varies considerably depending on the considered heat metric (particularly in Barcelona, Oslo, Lisbon, Warsaw, and Berlin; Figure 4), indicating that the choice of metrics may strongly influence projections of ambient heat in these cities. Additionally, in some cities the projections vary considerably within a box of 3x3 grid cells around the city centre (Supplementary Figure S4), especially for TX exceedances above 30 °C and HWMId-TX. The variability is generally largest for cities located close to the sea, particularly for HWMId-TX. This is related to the fact that HWMId-TX values are generally much higher over the sea than on land, which is mostly due to the low climatological variability of TXx over the sea (Figure S5). If cities are located close to the sea, the estimated HWMId-TX values may thus strongly depend on how much of the grid cell located closest to the city centre is covered by land and on how much this land fraction varies across EURO-CORDEX models. In such cases, a more accurate representation of local interactions between land and sea would be necessary (e.g., higher spatial resolution, accurate representation of advection, consideration of humidity) to generate more robust projections of ambient heat.

https://doi.org/10.5194/nhess-2023-99
Preprint. Discussion started: 6 July 2023


Natural Hazards and Earth System Sciences
Discussions

The spatial patterns of the heat metrics can largely be explained by the local temperature climatology and its projected changes (see importance of climate factors in Figure 5), with varying importance of the single explanatory factors depending on the considered metric. The explanatory factors explain most of the spatial variability in TXx change and in TX exceedances above 30 °C but they only partly explain the spatial variability in HWMId-TX. The remaining unexplained variance of the heat metrics might be connected to the amplified increase of extreme temperatures (Seneviratne et al., 2016; Vogel et al., 2017) (we use summer mean TX as explanatory factor) or asymmetric changes in the temperature distributions (we use the symmetric standard deviation of TX as explanatory factor). For HWMId-TX, the relatively large unexplained variance might be specifically connected to the definition of HWMId, i.e., to the usage of a cut-off temperature to define heatwaves and to the standardisation based on the climatology of TXx. The same is the case for TX exceedances above 30 °C, which are generally non-linear due to the usage of the absolute threshold of 30 °C. Among the location factors, the latitude of a city is the most important factor for explaining the spatial variance, particularly for TX exceedances above 30 °C. Generally, the explained variance is lower for location factors than for climate factors, indicating that local climate does certainly not only depend on the coordinates and elevation of a location but also on other local factors, such as the predominant atmospheric circulation or local feedbacks (e.g., vegetation, soil moisture). As the contribution of the explanatory variables to the explained variance is quantified based on correlation analysis, definitive cause-effect chains cannot be deduced. Particularly for the climate factors, the results should thus rather be interpreted as an indication of the extent to which the calculated heat metrics are influenced by the underlying temperature distribution and its projected future change.

4.2 Limitations and potential improvements

The ~12.5 km spatial resolution of the EUR-11 simulations enables a much more detailed assessment of climate variability and climate change at the city-level compared to GCMs. Yet, urban temperatures usually exhibit large variability within a city, i.e., at scales that currently cannot be resolved by the 0.11° EURO-CORDEX ensemble. Urban-resolving climate modelling may provide a way forward to better quantify climate effects at scales resolving single neighbourhoods (Sharma et al., 2021; Hamdi et al., 2020), which would add valuable information for assessing the risk of heat stress due to climate change at scales relevant for local health authorities and city planners. To achieve this, an adequate representation of urban land surfaces in models is essential. Yet, several land surface modules of models in the 0.11° EURO-CORDEX ensemble do not have dedicated urban tiles or only employ a simplified representation of urban areas. The CORDEX Flagship Pilot Study on URBan environments and Regional Climate Change (URB-RCC) is tackling this issue and may provide important advancements for urban-resolving climate modelling in the medium term. Investing in the development of urban parameterisations might have further benefits, as their implementation in climate models may also affect regional climate outside the urban areas (Katzfey et al., 2020). The reanalysis ERA5-Land does not have a dedicated urban tile either, which makes it less suitable for analysing climate at city-level despite its high resolution of about 9 km. Moreover, the missing urban representation currently prevents the usage of ERA5-Land as a reference dataset for the application of bias adjustment to investigate urban climate. Climate data from E-OBS might reflect urban conditions to the extent weather stations are present in cities. However, weather stations are

https://doi.org/10.5194/nhess-2023-99
Preprint. Discussion started: 6 July 2023

574 located on grassland, and E-OBS might thus underestimate ambient heat in heavily sealed parts of cities, such as city centres,
575 inner-city residential areas, or industrial zones. In case data from paired weather stations inside a city and in its rural
576 surroundings are available, a bias adjustment procedure for urban areas developed by Burgstall et al. (2021) can be applied to
577 adjust climate model data to urban conditions.
578 In our analysis, we do not find any pronounced UHI effects (Figure 3, Supplementary Figure S2), which is likely related to the
579 incomplete representation of urban areas in RCMs. As UHI is projected to only intensify gradually due to global warming
580 (Huang et al., 2019; Koomen and Diogo, 2017), our results for TXx change and HWMId should not be affected much by the
581 lack of UHI. However, the estimated exceedance rates of TX>30 °C and TN>20 °C would be impacted by UHI as they rely
582 on absolute temperature thresholds. As UHI might be elevated during heatwaves (Ward et al., 2016), ambient heat could be
583 underestimated if urban areas are not well represented in land surface modules. In addition, cities also differ in other parameters
584 and variables, such as roughness length and soil moisture, from the land cover that models currently use in urban areas, which
585 might affect our results beyond UHI.
586 Differences in climate forcing or process implementation between the CMIP5, CMIP6, and EURO-CORDEX ensembles, such
587 as differences in aerosol forcing (Boé et al., 2020; Gutiérrez et al., 2020; Nabat et al., 2020), or diverging trends in cloudiness
588 (Bartók et al., 2017), might further explain discrepancies in climate projections (Taranu et al., 2022). Additionally, several
589 EURO-CORDEX models do not consider plant physiological CO_2 effects and thus likely underestimate extreme temperatures
590 (Schwingshackl et al., 2019). Although the latter effect is confined to vegetated surfaces and should thus be less relevant in
591 heavily sealed urban areas, it might still influence urban temperatures if the land cover currently used by RCMs in urban areas
592 includes vegetation. This might partly explain the lower ambient heat projections of the EURO-CORDEX ensemble compared
593 to the CMIP5 and CMIP6 ensembles, particularly in eastern and northern Europe.
594 The usage of absolute thresholds for estimating the number of exceedance days (i.e., 30 °C for daily maximum temperatures
595 and 20 °C for daily minimum temperatures) does not reflect that temperatures vary considerably across European cities.
596 Consequently, the number of exceedance days differs substantially across cities, showing a strong gradient from southern to
597 northern European cities. While absolute temperature thresholds are a common metric used for projections of ambient heat
598 (e.g., Schwingshackl et al., 2021; Zhao et al., 2015; Kjellstrom et al., 2009; Casanueva et al., 2020), epidemiological studies
599 show continuous increases in health impacts above the locally optimal temperature (i.e., the temperature where minimal effects
600 of health outcomes are observed, Gasparrini et al., 2015). Moreover, epidemiological studies increasingly use the temperature
601 percentile instead of absolute temperatures as exposure metric to better reflect local conditions (Masselot et al., 2023).

602 **5 Conclusions**

603 EURO-CORDEX simulations at 0.11° resolution (EUR-11, ~12.5 km) deliver climate data for Europe at a resolution that is
604 high enough to analyse projections of ambient heat at the city-level (Figure 1). The temperature distributions of the EURO-
605 CORDEX models generally agree with data from ERA5-Land and E-OBS in the 36 major European cities investigated, despite

https://doi.org/10.5194/nhess-2023-99
Preprint. Discussion started: 6 July 2023

of a slight TX warm bias compared to ERA5, a slight TX cold bias compared to E-OBS, and a TN cold bias relative to both ERA5-Land and E-OBS (Figure 3, Supplementary Figure S2).

Using three different metrics to quantify ambient heat at 3 °C warming in Europe relative to 1981-2010 (i.e., changes in TXx, number of days with temperatures exceeding 30 °C, and HWMId), we find that ambient heat is projected to increase throughout the 36 major European cities investigated. Southern European cities will be particularly affected by high levels of ambient heat, but depending on the considered metric, cities in central, eastern, and northern Europe may also experience substantial increases in ambient heat (Figure 4). Nighttime HWMId increases even more strongly than daytime HWMId (Figure 6), with potentially severe implications for health (He et al., 2022). In several cities, the projected levels of ambient heat strongly depend on the considered metric, such as in Barcelona, Oslo, Lisbon, and Warsaw. This indicates that estimates based on a single metric might not appropriately reflect the risks of adverse health effects due to ambient heat in a warmer climate.

We further analyse the spatial patterns of the ambient heat projections in light of the underlying temperature climatology and its projected changes and the location of the different cities (Figure 5). Changes in TXx are mostly connected to projected changes in the mean and variability of TX, TX exceedances above 30 °C depend mostly on the average TX value in the reference period and its projected change, and the spatial patterns of HWMId are partly explained by changes in TX and the variability in the reference period. Regarding the location of cities, latitude plays the predominant role for explaining the spatial patterns, while the other factors (longitude, elevation, location close to sea) only have limited explanatory power.

The EURO-CORDEX ensemble estimates lower increases in TXx and lower HWMId values than the CMIP5 and CMIP6 ensembles in the majority of the analysed cities at 3 °C European warming (Figure 7). Yet, the EURO-CORDEX ensemble has higher TX exceedance rates of 30 °C in several cities, particularly in southern Europe. This discrepancy can be due to several factors, such as differences in forcing (Boé et al., 2020; Gutiérrez et al., 2020; Nabat et al., 2020), differences in process implementation (e.g., Bartók et al., 2017; Schwingshackl et al., 2019; Taranu et al., 2022), or the higher spatial resolution of EURO-CORDEX models being able to better represent local climate conditions. Yet, several EURO-CORDEX models do not represent urban areas, and the specific climate conditions in urban areas might thus not be fully represented.

The large ensemble of 72 EURO-CORDEX simulations enables a thorough uncertainty assessment, quantified by the spread across models. The uncertainties of TXx change are generally relatively low (around 1 °C to 2 °C in all cities). For TX exceedances above 30 °C, relative uncertainties range from 20% to 60% in most southern European cities but are higher in northern European cities due to their lower TX exceedance rates of 30 °C. Applying a simple bias adjustment (see Section 2.3) reduces the uncertainties of the projected TX exceedances above 30 °C in all cities and yields lower exceedance rates in about 40% of the cities. The estimates of ambient heat show high spatial variability around the city centre in cities located close to the shore. Particularly for HWMId, the estimates differ substantially depending on the presence of water or land in the respective grid cell (Supplementary Figure S4). Accurate representations of land and sea and of their interplay are thus essential for quantifying ambient heat in coastal cities.

Our analysis provides an important contribution to estimate ambient heat in 36 major European cities by considering three different metrics and using data from high-resolution RCM simulations. Future studies would benefit from a more

https://doi.org/10.5194/nhess-2023-99
Preprint. Discussion started: 6 July 2023

comprehensive representation of urban areas in models, which might be developed by the CORDEX Flagship Pilot Study on URBan environments and Regional Climate Change (URB-RCC) for RCMs. Systematically and completely including urban tiles in the land surface modules of the EURO-CORDEX RCMs and in ERA5-Land would allow for an even more accurate estimation of ambient heat at the city-level. Further, the coupling of urban models with regional climate models might pave the way for detailed analyses of heat stress in cities by combining the high spatial resolution of urban models with the climate variability estimates from RCMs. Such an analysis could provide an important step forward towards a comprehensive analysis of ambient heat in European cities, which could be combined with estimates of exposure and vulnerability to comprehensively quantify future risk of heat extremes.

Cities are expected to increasingly become climate hotspots due to their high population density and the local climate conditions that are partly influenced by how cities are structured. At the same time, their large innovation potential also gives cities the opportunity to lead the way in implementing climate adaptation strategies. Providing detailed and accurate data about ambient heat projections at the city-level is essential to enable cities to plan specific and effective adaptation measures against future heat extremes.

Code availability

The programming code used for the analyses and for creating the figures is available on https://github.com/schwings-clemens/ambient-heat-european-cities.

Data availability

Data supporting this study is publicly available from https://doi.org/10.5281/zenodo.8043755. EURO-CORDEX, CMIP5, and CMIP6 data is available via the Earth System Grid Federation (ESGF) and can be downloaded from https://esgf-data.dkrz.de. ERA5-Land is available from https://doi.org/10.24381/cds.e2161bac. E-OBS is available from https://doi.org/10.24381/cds.151d3ec6. Weather station data from GSOD can be retrieved from https://data.nodc.noaa.gov/cgi-bin/iso?id=gov.noaa.ncdc:C00516 and weather station data from ECA&D can be retrieved from https://www.ecad.eu.

Author contribution

CS and JS conceptualised the study. CI and CS curated the data. CS developed the methodology, performed the analysis, and created the visualisations. JS and KA acquired funding. CS and AD drafted the manuscript. CS, AD, CI, KA, and JS edited and wrote the manuscript.

https://doi.org/10.5194/nhess-2023-99
Preprint. Discussion started: 6 July 2023

668 **Competing interests**

669 The authors declare that they have no conflict of interest.

670 **Acknowledgments**

671 We thank Nina Schuhen for her support with the statistical analysis, particularly regarding the quantification of how much the
672 different explanatory factors can explain the observed spatial patterns of ambient heat. We further thank Marit Sandstad for
673 processing the ERA5-Land data. We acknowledge the E-OBS dataset and the data providers in the ECA&D project
674 (https://www.ecad.eu). This study contains modified Copernicus Climate Change Service information [2022]. We
675 acknowledge the World Climate Research Programme's Working Group on Coupled Modelling, which is responsible for
676 CMIP, the World Climate Research Programme's Working Group on Regional Climate, and the Working Group on Coupled
677 Modelling, former coordinating body of CORDEX and responsible panel for CMIP5. We thank the climate modelling groups
678 for producing and making available their model output, the Earth System Grid Federation (ESGF) for archiving the data and
679 providing access, and the multiple funding agencies who support CMIP5, CMIP6 and ESGF. We also acknowledge the Earth
680 System Grid Federation infrastructure, an international effort led by the US Department of Energy's Program for Climate
681 Model Diagnosis and Intercomparison, the European Network for Earth System Modelling and other partners in the Global
682 Organisation for Earth System Science Portals (GO-ESSP). For CMIP the US Department of Energy's Program for Climate
683 Model Diagnosis and Intercomparison provides coordinating support and led development of software infrastructure in
684 partnership with the Global Organization for Earth System Science Portals.
685 This work has received funding from the European Union's Horizon 2020 research and innovation program under grant
686 agreement No 820655 (EXHAUSTION) and from the Belmont Forum Collaborative Research Action on Climate,
687 Environment, and Health, supported by the Research Council of Norway (contract No 310672, HEATCOST). Jana Sillmann
688 and Anne Sophie Daloz were supported through the CICERO Strategic Project on Climate Change Risk (no. 160015/F40),
689 funded by the Research Council of Norway.
690

https://doi.org/10.5194/nhess-2023-99
Preprint. Discussion started: 6 July 2023

References

Alizadeh, M. R., Abatzoglou, J. T., Adamowski, J. F., Prestemon, J. P., Chittoori, B., Akbari Asanjan, A., and Sadegh, M.: Increasing Heat-Stress Inequality in a Warming Climate, Earths Future, 10, https://doi.org/10.1029/2021EF002488, 2022.

Argueso, D., Evans, J. P., Pitman, A. J., and Di Luca, A.: Effects of city expansion on heat stress under climate change conditions, PLOS ONE, 10, e0117066, https://doi.org/10.1371/journal.pone.0117066, 2015.

Åström, D. O., Forsberg, B., Edvinsson, S., and Rocklöv, J.: Acute Fatal Effects of Short-Lasting Extreme Temperatures in Stockholm, Sweden: Evidence Across a Century of Change, Epidemiology, 24, 820–829, https://doi.org/10.1097/01.ede.0000434530.62353.0b, 2013.

Azen, R. and Budescu, D. V.: The dominance analysis approach for comparing predictors in multiple regression., Psychol. Methods, 8, 129–129, https://doi.org/10.1037/1082-989X.8.2.129, 2003.

Bartók, B., Wild, M., Folini, D., Lüthi, D., Kotlarski, S., Schär, C., Vautard, R., Jerez, S., and Imecs, Z.: Projected changes in surface solar radiation in CMIP5 global climate models and in EURO-CORDEX regional climate models for Europe, Clim. Dyn., 49, 2665-2683-2665–2683, https://doi.org/10.1007/s00382-016-3471-2, 2017.

Boé, J., Somot, S., Corre, L., and Nabat, P.: Large discrepancies in summer climate change over Europe as projected by global and regional climate models: causes and consequences, Clim. Dyn., 54, 2981–3002, https://doi.org/10.1007/s00382-020-05153-1, 2020.

Burgstall, A., Kotlarski, S., Casanueva, A., Hertig, E., Fischer, E., and Knutti, R.: Urban multi-model climate projections of intense heat in Switzerland, Clim. Serv., 22, 100228, https://doi.org/10.1016/j.cliser.2021.100228, 2021.

Casanueva, A., Kotlarski, S., Fischer, A. M., Flouris, A. D., Kjellstrom, T., Lemke, B., Nybo, L., Schwierz, C., and Liniger, M. A.: Escalating environmental summer heat exposure—a future threat for the European workforce, Reg. Environ. Change, 20, https://doi.org/10.1007/s10113-020-01625-6, 2020.

Chapman, S., Thatcher, M., Salazar, A., Watson, J. E. M., and McAlpine, C. A.: The impact of climate change and urban growth on urban climate and heat stress in a subtropical city, Int. J. Climatol., 39, 3013–3030, https://doi.org/10.1002/joc.5998, 2019.

Coppola, E., Nogherotto, R., Ciarlo, J. M., Giorgi, F., Meijgaard, E., Kadygrov, N., Iles, C., Corre, L., Sandstad, M., Somot, S., Nabat, P., Vautard, R., Levavasseur, G., Schwingshackl, C., Sillmann, J., Kjellström, E., Nikulin, G., Aalbers, E., Lenderink, G., Christensen, O. B., Boberg, F., Sørland, S. L., Demory, M.-E., Bülow, K., Teichmann, C., Warrach-Sagi, K., and Wulfmeyer, V.: Assessment of the European Climate Projections as Simulated by the Large EURO-CORDEX Regional and Global Climate Model Ensemble, J. Geophys. Res. Atmospheres, 126, https://doi.org/10.1029/2019jd032356, 2021.

Cornes, R. C., van der Schrier, G., van den Besselaar, E. J. M., and Jones, P. D.: An Ensemble Version of the E-OBS Temperature and Precipitation Data Sets, J. Geophys. Res. Atmospheres, 123, 9391–9409, https://doi.org/10.1029/2017jd028200, 2018.

Dosio, A., Mentaschi, L., Fischer, E. M., and Wyser, K.: Extreme heat waves under 1.5 °C and 2 °C global warming, Environ. Res. Lett., 13, 054006, https://doi.org/10.1088/1748-9326/aab827, 2018.

Fischer, E. M. and Schär, C.: Consistent geographical patterns of changes in high-impact European heatwaves, Nat. Geosci., 3, 398–398, https://doi.org/10.1038/ngeo866, 2010.

https://doi.org/10.5194/nhess-2023-99
Preprint. Discussion started: 6 July 2023

Forzieri, G., Feyen, L., Russo, S., Vousdoukas, M., Alfieri, L., Outten, S., Migliavacca, M., Bianchi, A., Rojas, R., and Cid, A.: Multi-hazard assessment in Europe under climate change, Clim. Change, 137, 105–119, https://doi.org/10.1007/s10584-016-1661-x, 2016.

Freychet, N., Hegerl, G. C., Lord, N. S., Lo, Y. T. E., Mitchell, D., and Collins, M.: Robust increase in population exposure to heat stress with increasing global warming, Environ. Res. Lett., 17, 064049, https://doi.org/10.1088/1748-9326/ac71b9, 2022.

García-León, D., Casanueva, A., Standardi, G., Burgstall, A., Flouris, A. D., and Nybo, L.: Current and projected regional economic impacts of heatwaves in Europe, Nat. Commun., 12, 5807, https://doi.org/10.1038/s41467-021-26050-z, 2021.

Gasparrini, A., Guo, Y., Hashizume, M., Lavigne, E., Zanobetti, A., Schwartz, J., Tobias, A., Tong, S., Rocklöv, J., Forsberg, B., Leone, M., De Sario, M., Bell, M. L., Guo, Y.-L. L., Wu, C., Kan, H., Yi, S.-M., de Sousa Zanotti Stagliorio Coelho, M., Saldiva, P. H. N., Honda, Y., Kim, H., and Armstrong, B.: Mortality risk attributable to high and low ambient temperature: a multicountry observational study, The Lancet, 386, 369–375, https://doi.org/10.1016/S0140-6736(14)62114-0, 2015.

Gasparrini, A., Guo, Y., Sera, F., Vicedo-Cabrera, A. M., Huber, V., Tong, S., de Sousa Zanotti Stagliorio Coelho, M., Saldiva, P. H. N., Lavigne, E., Correa, P. M., Ortega, N. V., Kan, H., Osorio, S., Kyselý, J., Urban, A., Jaakkola, J. J. K., Ryti, N. R. I., Pascal, M., Goodman, P. G., Zeka, A., Michelozzi, P., Scortichini, M., Hashizume, M., Honda, Y., Hurtado-Diaz, M., Cruz, J. C., Seposo, X., Kim, H., Tobias, A., Iñiguez, C., Forsberg, B., Åström, D. O., Ragettli, M. S., Guo, Y. L., Wu, C., Zanobetti, A., Schwartz, J., Bell, M. L., Dang, T. N., Van, D. D., Heaviside, C., Vardoulakis, S., Hajat, S., Haines, A., and Armstrong, B.: Projections of temperature-related excess mortality under climate change scenarios, Lancet Planet. Health, 1, e360-e367-e360–e367, https://doi.org/10.1016/S2542-5196(17)30156-0, 2017.

Goret, M., Masson, V., Schoetter, R., and Moine, M.-P.: Inclusion of CO2 flux modelling in an urban canopy layer model and an evaluation over an old European city centre, Atmospheric Environ. X, 3, 100042, https://doi.org/10.1016/j.aeaoa.2019.100042, 2019.

Guerreiro, S. B., Dawson, R. J., Kilsby, C., Lewis, E., and Ford, A.: Future heat-waves, droughts and floods in 571 European cities, Environ. Res. Lett., 13, https://doi.org/10.1088/1748-9326/aaaad3, 2018.

Gutiérrez, C., Somot, S., Nabat, P., Mallet, M., Corre, L., Meijgaard, E. van, Perpiñán, O., and Gaertner, M. Á.: Future evolution of surface solar radiation and photovoltaic potential in Europe: investigating the role of aerosols, Environ. Res. Lett., 15, 034035, https://doi.org/10.1088/1748-9326/ab6666, 2020.

Hamdi, R., Kusaka, H., Doan, Q.-V., Cai, P., He, H., Luo, G., Kuang, W., Caluwaerts, S., Duchêne, F., Van Schaeybroek, B., and Termonia, P.: The State-of-the-Art of Urban Climate Change Modeling and Observations, Earth Syst. Environ., 4, 631–646, https://doi.org/10.1007/s41748-020-00193-3, 2020.

He, C., Kim, H., Hashizume, M., Lee, W., Honda, Y., Kim, S. E., Kinney, P. L., Schneider, A., Zhang, Y., Zhu, Y., Zhou, L., Chen, R., and Kan, H.: The effects of night-time warming on mortality burden under future climate change scenarios: a modelling study, Lancet Planet. Health, 6, e648–e657, https://doi.org/10.1016/S2542-5196(22)00139-5, 2022.

Heaviside, C., Macintyre, H., and Vardoulakis, S.: The Urban Heat Island: Implications for Health in a Changing Environment, Curr Env. Health Rep, 4, 296–305, https://doi.org/10.1007/s40572-017-0150-3, 2017.

Huang, K., Li, X., Liu, X., and Seto, K. C.: Projecting global urban land expansion and heat island intensification through 2050, Environ. Res. Lett., 14, 114037, https://doi.org/10.1088/1748-9326/ab4b71, 2019.

https://doi.org/10.5194/nhess-2023-99
Preprint. Discussion started: 6 July 2023

Iles, C. E., Vautard, R., Strachan, J., Joussaume, S., Eggen, B. R., and Hewitt, C. D.: The benefits of increasing resolution in global and regional climate simulations for European climate extremes, Geosci. Model Dev., 13, 5583–5607, https://doi.org/10.5194/gmd-13-5583-2020, 2020.

IPCC: Climate Change 2021: The Physical Science Basis. Contribution of Working Group I to the Sixth Assessment Report of the Intergovernmental Panel on Climate Change, Cambridge University Press, Cambridge, United Kingdom and New York, NY, USA, 2021.

IPCC: Climate Change 2022: Impacts, Adaptation and Vulnerability. Contribution of Working Group II to the Sixth Assessment Report of the Intergovernmental Panel on Climate Change, edited by: H.-O. Pörtner, B. R., D. C. Roberts, M. Tignor, E. S. Poloczanska, K. Mintenbeck, A. Alegría, M. Craig, S. Langsdorf, S. Löschke, V. Möller, A. Okem, Cambridge University Press, Cambridge, UK and New York, NY, USA, https://doi.org/10.1017/9781009325844.001, 2022.

Jacob, D., Petersen, J., Eggert, B., Alias, A., Christensen, O. B., Bouwer, L. M., Braun, A., Colette, A., Déqué, M., Georgievski, G., Georgopoulou, E., Gobiet, A., Menut, L., Nikulin, G., Haensler, A., Hempelmann, N., Jones, C., Keuler, K., Kovats, S., Kröner, N., Kotlarski, S., Kriegsmann, A., Martin, E., van Meijgaard, E., Moseley, C., Pfeifer, S., Preuschmann, S., Radermacher, C., Radtke, K., Rechid, D., Rounsevell, M., Samuelsson, P., Somot, S., Soussana, J.-F., Teichmann, C., Valentini, R., Vautard, R., Weber, B., and Yiou, P.: EURO-CORDEX: new high-resolution climate change projections for European impact research, Reg. Environ. Change, 14, 563–578, https://doi.org/10.1007/s10113-013-0499-2, 2013.

Junk, J., Goergen, K., and Krein, A.: Future Heat Waves in Different European Capitals Based on Climate Change Indicators, Int J Env. Res Public Health, 16, https://doi.org/10.3390/ijerph16203959, 2019.

Karwat, A. and Franzke, C. L. E.: Future Projections of Heat Mortality Risk for Major European Cities, Weather Clim. Soc., https://doi.org/10.1175/WCAS-D-20-0142.1, 2021.

Katzfey, J., Schlünzen, H., Hoffmann, P., and Thatcher, M.: How an urban parameterization affects a high-resolution global climate simulation, Q. J. R. Meteorol. Soc., 146, 3808–3829, https://doi.org/10.1002/qj.3874, 2020.

Keat, W. J., Kendon, E. J., and Bohnenstengel, S. I.: Climate change over UK cities: the urban influence on extreme temperatures in the UK climate projections, Clim. Dyn., 57, 3583–3597, https://doi.org/10.1007/s00382-021-05883-w, 2021.

Kjellstrom, T., Kovats, R. S., Lloyd, S. J., Holt, T., and Tol, R. S. J.: The Direct Impact of Climate Change on Regional Labor Productivity, Arch. Environ. Occup. Health, 64, 217-227-217–227, https://doi.org/10.1080/19338240903352776, 2009.

Klein Tank, A. M. G., Wijngaard, J. B., Können, G. P., Böhm, R., Demarée, G., Gocheva, A., Mileta, M., Pashiardis, S., Hejkrlik, L., Kern-Hansen, C., Heino, R., Bessemoulin, P., Müller-Westermeier, G., Tzanakou, M., Szalai, S., Pálsdóttir, T., Fitzgerald, D., Rubin, S., Capaldo, M., Maugeri, M., Leitass, A., Bukantis, A., Aberfeld, R., van Engelen, A. F. V., Forland, E., Mietus, M., Coelho, F., Mares, C., Razuvaev, V., Nieplova, E., Cegnar, T., Antonio López, J., Dahlström, B., Moberg, A., Kirchhofer, W., Ceylan, A., Pachaliuk, O., Alexander, L. V., and Petrovic, P.: Daily dataset of 20th-century surface air temperature and precipitation series for the European Climate Assessment, Int. J. Climatol., 22, 1441–1453, https://doi.org/10.1002/joc.773, 2002.

Klok, E. J. and Klein Tank, A. M. G.: Updated and extended European dataset of daily climate observations, Int. J. Climatol., 29, 1182–1191, https://doi.org/10.1002/joc.1779, 2009.

Koomen, E. and Diogo, V.: Assessing potential future urban heat island patterns following climate scenarios, socio-economic developments and spatial planning strategies, Mitig. Adapt. Strateg. Glob. Change, 22, 287–306, https://doi.org/10.1007/s11027-015-9646-z, 2017.

https://doi.org/10.5194/nhess-2023-99
Preprint. Discussion started: 6 July 2023

Krayenhoff, E. S., Jiang, T., Christen, A., Martilli, A., Oke, T. R., Bailey, B. N., Nazarian, N., Voogt, J. A., Giometto, M. G., Stastny, A., and Crawford, B. R.: A multi-layer urban canopy meteorological model with trees (BEP-Tree): Street tree impacts on pedestrian-level climate, Urban Clim., 32, 100590, https://doi.org/10.1016/j.uclim.2020.100590, 2020.

Kusaka, H., Hara, M., and Takane, Y.: Urban Climate Projection by the WRF Model at 3-km Horizontal Grid Increment: Dynamical Downscaling and Predicting Heat Stress in the 2070's August for Tokyo, Osaka, and Nagoya Metropolises, J. Meteorol. Soc. Jpn. Ser II, 90B, 47–63, https://doi.org/10.2151/jmsj.2012-B04, 2012.

Langendijk, G. S., Rechid, D., and Jacob, D.: Urban Areas and Urban–Rural Contrasts under Climate Change: What Does the EURO-CORDEX Ensemble Tell Us?—Investigating near Surface Humidity in Berlin and Its Surroundings, Atmosphere, 10, https://doi.org/10.3390/atmos10120730, 2019.

Li, C., Zwiers, F., Zhang, X., Li, G., Sun, Y., and Wehner, M.: Changes in Annual Extremes of Daily Temperature and Precipitation in CMIP6 Models, J. Clim., 34, 3441–3460, https://doi.org/10.1175/JCLI-D-19-1013.1, 2021.

Li, D. and Bou-Zeid, E.: Synergistic Interactions between Urban Heat Islands and Heat Waves: The Impact in Cities Is Larger than the Sum of Its Parts, J. Appl. Meteorol. Climatol., 52, 2051–2064, https://doi.org/10.1175/jamc-d-13-02.1, 2013.

Lin, C., Kjellström, E., Wilcke, R. A. I., and Chen, D.: Present and future European heat wave magnitudes: climatologies, trends, and their associated uncertainties in GCM-RCM model chains, Earth Syst. Dyn., 13, 1197–1214, https://doi.org/10.5194/esd-13-1197-2022, 2022.

Lundgren, K., Kuklane, K., Gao, C., and HOLM^|^Eacute;R, I.: Effects of Heat Stress on Working Populations when Facing Climate Change, Ind. Health, 51, 3–15, https://doi.org/10.2486/indhealth.2012-0089, 2013.

Maraun, D.: Bias Correcting Climate Change Simulations - a Critical Review, Curr. Clim. Change Rep., 2, 211-220-211–220, https://doi.org/10.1007/s40641-016-0050-x, 2016.

Masselot, P., Mistry, M., Vanoli, J., Schneider, R., Iungman, T., Garcia-Leon, D., Ciscar, J.-C., Feyen, L., Orru, H., Urban, A., Breitner, S., Huber, V., Schneider, A., Samoli, E., Stafoggia, M., de'Donato, F., Rao, S., Armstrong, B., Nieuwenhuijsen, M., Vicedo-Cabrera, A. M., Gasparrini, A., Achilleos, S., Kyselý, J., Indermitte, E., Jaakkola, J. J. K., Ryti, N., Pascal, M., Katsouyanni, K., Analitis, A., Goodman, P., Zeka, A., Michelozzi, P., Houthuijs, D., Ameling, C., Rao, S., das Neves Pereira da Silva, S., Madureira, J., Holobaca, I.-H., Tobias, A., Íñiguez, C., Forsberg, B., Åström, C., Ragettli, M. S., Analitis, A., Katsouyanni, K., Surname, F. name, Zafeiratou, S., Vazquez Fernandez, L., Monteiro, A., Rai, M., Zhang, S., and Aunan, K.: Excess mortality attributed to heat and cold: a health impact assessment study in 854 cities in Europe, Lancet Planet. Health, 7, e271–e281, https://doi.org/10.1016/S2542-5196(23)00023-2, 2023.

Masson, V., Lemonsu, A., Hidalgo, J., and Voogt, J.: Urban Climates and Climate Change, Annu. Rev. Environ. Resour., 45, 411–444, https://doi.org/10.1146/annurev-environ-012320-083623, 2020.

McMichael, A. J., Woodruff, R. E., and Hales, S.: Climate change and human health: present and future risks, The Lancet, 367, 859-869-859–869, https://doi.org/10.1016/S0140-6736(06)68079-3, 2006.

Molina, M. O., Sanchez, E., and Gutierrez, C.: Future heat waves over the Mediterranean from an Euro-CORDEX regional climate model ensemble, Sci Rep, 10, 8801, https://doi.org/10.1038/s41598-020-65663-0, 2020.

Muñoz-Sabater, J., Dutra, E., Agustí-Panareda, A., Albergel, C., Arduini, G., Balsamo, G., Boussetta, S., Choulga, M., Harrigan, S., Hersbach, H., Martens, B., Miralles, D. G., Piles, M., Rodríguez-Fernández, N. J., Zsoter, E., Buontempo, C., and Thépaut, J.-N.: ERA5-Land: a state-of-the-art global reanalysis dataset for land applications, Earth Syst. Sci. Data, 13, 4349–4383, https://doi.org/10.5194/essd-13-4349-2021, 2021.

https://doi.org/10.5194/nhess-2023-99
Preprint. Discussion started: 6 July 2023

839 Nabat, P., Somot, S., Cassou, C., Mallet, M., Michou, M., Bouniol, D., Decharme, B., Drugé, T., Roehrig, R., and Saint-
840 Martin, D.: Modulation of radiative aerosols effects by atmospheric circulation over the Euro-Mediterranean region,
841 Atmospheric Chem. Phys., 20, 8315–8349, https://doi.org/10.5194/acp-20-8315-2020, 2020.

842 Orlov, A., Daloz, A. S., Sillmann, J., Thiery, W., Douzal, C., Lejeune, Q., and Schleussner, C.: Global Economic Responses
843 to Heat Stress Impacts on Worker Productivity in Crop Production, Econ. Disasters Clim. Change, 5, 367–390,
844 https://doi.org/10.1007/s41885-021-00091-6, 2021.

845 Perkins, S. E.: A review on the scientific understanding of heatwaves—Their measurement, driving mechanisms, and changes
846 at the global scale, Atmospheric Res., 164–165, 242-267-242–267, https://doi.org/10.1016/j.atmosres.2015.05.014, 2015.

847 Perkins, S. E. and Alexander, L. V.: On the Measurement of Heat Waves, J. Clim., 26, 4500–4517,
848 https://doi.org/10.1175/JCLI-D-12-00383.1, 2013.

849 Perkins-Kirkpatrick, S. E. and Lewis, S. C.: Increasing trends in regional heatwaves, Nat. Commun., 11, 3357,
850 https://doi.org/10.1038/s41467-020-16970-7, 2020.

851 Petkova, E. P., Gasparrini, A., and Kinney, P. L.: Heat and Mortality in New York City Since the Beginning of the 20th
852 Century:, Epidemiology, 25, 554–560, https://doi.org/10.1097/EDE.0000000000000123, 2014.

853 Ramamurthy, P. and Bou-Zeid, E.: Heatwaves and urban heat islands: A comparative analysis of multiple cities, J. Geophys.
854 Res. Atmospheres, 122, 168–178, https://doi.org/10.1002/2016jd025357, 2017.

855 Royé, D., Sera, F., Tobías, A., Lowe, R., Gasparrini, A., Pascal, M., de'Donato, F., Nunes, B., and Teixeira, J. P.: Effects of
856 Hot Nights on Mortality in Southern Europe, Epidemiology, 32, 487–498, https://doi.org/10.1097/EDE.0000000000001359,
857 2021.

858 Russo, S., Sillmann, J., and Fischer, E. M.: Top ten European heatwaves since 1950 and their occurrence in the coming decades,
859 Environ. Res. Lett., 10, https://doi.org/10.1088/1748-9326/10/12/124003, 2015.

860 Russo, S., Sillmann, J., and Sterl, A.: Humid heat waves at different warming levels, Sci. Rep., 7, 7477–7477,
861 https://doi.org/10.1038/s41598-017-07536-7, 2017.

862 Schwingshackl, C., Hirschi, M., and Seneviratne, S. I.: Global Contributions of Incoming Radiation and Land Surface
863 Conditions to Maximum Near-Surface Air Temperature Variability and Trend, Geophys Res Lett, 45, 5034–5044,
864 https://doi.org/10.1029/2018GL077794, 2018.

865 Schwingshackl, C., Davin, E. L., Hirschi, M., Sørland, S. L., Wartenburger, R., and Seneviratne, S. I.: Regional climate model
866 projections underestimate future warming due to missing plant physiological CO2 response, Environ. Res. Lett., 14,
867 https://doi.org/10.1088/1748-9326/ab4949, 2019.

868 Schwingshackl, C., Sillmann, J., Vicedo-Cabrera, A. M., Sandstad, M., and Aunan, K.: Heat Stress Indicators in CMIP6:
869 Estimating Future Trends and Exceedances of Impact-Relevant Thresholds, Earths Future, 9,
870 https://doi.org/10.1029/2020ef001885, 2021.

871 Seneviratne, S. I. and Hauser, M.: Regional Climate Sensitivity of Climate Extremes in CMIP6 Versus CMIP5 Multimodel
872 Ensembles, Earths Future, 8, https://doi.org/10.1029/2019EF001474, 2020.

873 Seneviratne, S. I., Donat, M. G., Pitman, A. J., Knutti, R., and Wilby, R. L.: Allowable CO2 emissions based on regional and
874 impact-related climate targets, Nature, 529, 477–83, https://doi.org/10.1038/nature16542, 2016.

https://doi.org/10.5194/nhess-2023-99
Preprint. Discussion started: 6 July 2023

Sera, F., Armstrong, B., Tobias, A., Vicedo-Cabrera, A. M., Åström, C., Bell, M. L., Chen, B.-Y., de Sousa Zanotti Stagliorio Coelho, M., Matus Correa, P., Cruz, J. C., Dang, T. N., Hurtado-Diaz, M., Do Van, D., Forsberg, B., Guo, Y. L., Guo, Y., Hashizume, M., Honda, Y., Iñiguez, C., Jaakkola, J. J. K., Kan, H., Kim, H., Lavigne, E., Michelozzi, P., Ortega, N. V., Osorio, S., Pascal, M., Ragettli, M. S., Ryti, N. R. I., Saldiva, P. H. N., Schwartz, J., Scortichini, M., Seposo, X., Tong, S., Zanobetti, A., and Gasparrini, A.: How urban characteristics affect vulnerability to heat and cold: a multi-country analysis, Int. J. Epidemiol., 48, 1101–1112, https://doi.org/10.1093/ije/dyz008, 2019.

Sharma, A., Wuebbles, D. J., and Kotamarthi, R.: The Need for Urban-Resolving Climate Modeling Across Scales, AGU Adv., 2, https://doi.org/10.1029/2020AV000271, 2021.

Sharma, R., Hooyberghs, H., Lauwaet, D., and De Ridder, K.: Urban Heat Island and Future Climate Change-Implications for Delhi's Heat, J Urban Health, 96, 235–251, https://doi.org/10.1007/s11524-018-0322-y, 2019.

Sillmann, J., Kharin, V. V., Zwiers, F. W., Zhang, X., and Bronaugh, D.: Climate extremes indices in the CMIP5 multimodel ensemble: Part 2. Future climate projections, J. Geophys. Res. Atmospheres, 118, 2473-2493-2473–2493, https://doi.org/10.1002/jgrd.50188, 2013.

Smid, M., Russo, S., Costa, A. C., Granell, C., and Pebesma, E.: Ranking European capitals by exposure to heat waves and cold waves, Urban Clim., 27, 388–402, https://doi.org/10.1016/j.uclim.2018.12.010, 2019.

Smith, A., Lott, N., and Vose, R.: The Integrated Surface Database: Recent Developments and Partnerships, Bull. Am. Meteorol. Soc., 92, 704–708, https://doi.org/10.1175/2011bams3015.1, 2011.

Suarez-Gutierrez, L., Müller, W. A., Li, C., and Marotzke, J.: Dynamical and thermodynamical drivers of variability in European summer heat extremes, Clim. Dyn., 54, 4351–4366, https://doi.org/10.1007/s00382-020-05233-2, 2020.

Sunyer, M. A., Hundecha, Y., Lawrence, D., Madsen, H., Willems, P., Martinkova, M., Vormoor, K., Bürger, G., Hanel, M., Kriaučiūnienė, J., Loukas, A., Osuch, M., and Yücel, I.: Inter-comparison of statistical downscaling methods for projection of extreme precipitation in Europe, Hydrol. Earth Syst. Sci., 19, 1827–1847, https://doi.org/10.5194/hess-19-1827-2015, 2015.

Taranu, I. S., Somot, S., Alias, A., Boé, J., and Delire, C.: Mechanisms behind large-scale inconsistencies between regional and global climate model-based projections over Europe, Clim. Dyn., https://doi.org/10.1007/s00382-022-06540-6, 2022.

Thompson, R., Landeg, O., Kar-Purkayastha, I., Hajat, S., Kovats, S., and O'Connell, E.: Heatwave Mortality in Summer 2020 in England: An Observational Study, Int. J. Environ. Res. Public. Health, 19, 6123, https://doi.org/10.3390/ijerph19106123, 2022.

UN-Habitat: Cities and Climate Change, 0 ed., Routledge, https://doi.org/10.4324/9781849776936, 2011.

Vargas Zeppetello, L. R., Raftery, A. E., and Battisti, D. S.: Probabilistic projections of increased heat stress driven by climate change, Commun. Earth Environ., 3, 183, https://doi.org/10.1038/s43247-022-00524-4, 2022.

Vautard, R., Gobiet, A., Jacob, D., Belda, M., Colette, A., Déqué, M., Fernández, J., García-Díez, M., Goergen, K., Güttler, I., Halenka, T., Karacostas, T., Katragkou, E., Keuler, K., Kotlarski, S., Mayer, S., van Meijgaard, E., Nikulin, G., Patarčić, M., Scinocca, J., Sobolowski, S., Suklitsch, M., Teichmann, C., Warrach-Sagi, K., Wulfmeyer, V., and Yiou, P.: The simulation of European heat waves from an ensemble of regional climate models within the EURO-CORDEX project, Clim. Dyn., 41, 2555–2575, https://doi.org/10.1007/s00382-013-1714-z, 2013.

Vautard, R., Kadygrov, N., Iles, C., Boberg, F., Buonomo, E., Bülow, K., Coppola, E., Corre, L., Meijgaard, E., Nogherotto, R., Sandstad, M., Schwingshackl, C., Somot, S., Aalbers, E., Christensen, O. B., Ciarlo, J. M., Demory, M.-E., Giorgi, F.,

https://doi.org/10.5194/nhess-2023-99
Preprint. Discussion started: 6 July 2023

Jacob, D., Jones, R. G., Keuler, K., Kjellström, E., Lenderink, G., Levavasseur, G., Nikulin, G., Sillmann, J., Solidoro, C., Sørland, S. L., Steger, C., Teichmann, C., Warrach-Sagi, K., and Wulfmeyer, V.: Evaluation of the Large EURO-CORDEX Regional Climate Model Ensemble, J. Geophys. Res. Atmospheres, 126, https://doi.org/10.1029/2019jd032344, 2021.

Vogel, M. M., Orth, R., Cheruy, F., Hagemann, S., Lorenz, R., Hurk, B. J. J. M., and Seneviratne, S. I.: Regional amplification of projected changes in extreme temperatures strongly controlled by soil moisture-temperature feedbacks, Geophys. Res. Lett., 44, 1511-1519-1511–1519, https://doi.org/10.1002/2016GL071235, 2017.

Ward, K., Lauf, S., Kleinschmit, B., and Endlicher, W.: Heat waves and urban heat islands in Europe: A review of relevant drivers, Sci Total Env., 569–570, 527–539, https://doi.org/10.1016/j.scitotenv.2016.06.119, 2016.

Wartenburger, R., Hirschi, M., Donat, M. G., Greve, P., Pitman, A. J., and Seneviratne, S. I.: Changes in regional climate extremes as a function of global mean temperature: an interactive plotting framework, Geosci. Model Dev., 10, 3609–3634, https://doi.org/10.5194/gmd-10-3609-2017, 2017.

Wouters, H., De Ridder, K., Poelmans, L., Willems, P., Brouwers, J., Hosseinzadehtalaei, P., Tabari, H., Vanden Broucke, S., van Lipzig, N. P. M., and Demuzere, M.: Heat stress increase under climate change twice as large in cities as in rural areas: A study for a densely populated midlatitude maritime region, Geophys. Res. Lett., 44, 8997–9007, https://doi.org/10.1002/2017gl074889, 2017.

Yang, J., Zhou, M., Ren, Z., Li, M., Wang, B., Liu, D. L., Ou, C.-Q., Yin, P., Sun, J., Tong, S., Wang, H., Zhang, C., Wang, J., Guo, Y., and Liu, Q.: Projecting heat-related excess mortality under climate change scenarios in China, Nat. Commun., 12, 1039, https://doi.org/10.1038/s41467-021-21305-1, 2021.

Zhao, Y., Ducharne, A., Sultan, B., Braconnot, P., and Vautard, R.: Estimating heat stress from climate-based indicators: present-day biases and future spreads in the CMIP5 global climate model ensemble, Environ. Res. Lett., 10, 084013–084013, https://doi.org/10.1088/1748-9326/10/8/084013, 2015.

Zheng, Z., Zhao, L., and Oleson, K. W.: Large model structural uncertainty in global projections of urban heat waves, Nat Commun, 12, 3736, https://doi.org/10.1038/s41467-021-24113-9, 2021.

Zittis, G., Hadjinicolaou, P., Almazroui, M., Bucchignani, E., Driouech, F., El Rhaz, K., Kurnaz, L., Nikulin, G., Ntoumos, A., Ozturk, T., Proestos, Y., Stenchikov, G., Zaaboul, R., and Lelieveld, J.: Business-as-usual will lead to super and ultra-extreme heatwaves in the Middle East and North Africa, Npj Clim. Atmospheric Sci., 4, 20, https://doi.org/10.1038/s41612-021-00178-7, 2021.